Graduation Thesis

Electron Temperature Distribution in Quantum Hall Systems with Potential Steps

Yuki Nagai

Laboratory of Theoretical Solid State Physics
Condensed Matter Physics Division
Department of Applied Physics
Faculty of Engineering
Hokkaido University

March 9, 2005

Contents

Chapter 1

Introduction

1.1 Background

1.1.1 Two-Dimensional Electron Systems

Electrons and holes are generally free to move in all three spatial directions in bulk metals and semiconductors. If this freedom is restricted in certain directions, the dimensionality of the system becomes reduced. For example, in a two-dimensional system, the electrons can only move in one plane and may not travel perpendicular to this plane. An example of naturally occuring material showing quasi-2D behavior is graphite where the resistance measured along the sheets is much lower than between sheets. With an advanced technology on microfabrication, we can make two-dimensional electron systems(2DES) artificially.

1.1.2 Formation of Two-Dimensional Electron Systems

Molecular beam epitaxy(MBE) technique is one of the methods for the formation of two-dimensional electron systems. The formation of two-dimensional electron systems in GaAs-AlGaAs heterostructure is as follows. Electrons are in the AlGaAs conduction band since the part of the AlGaAs is doped n-type. These electrons move to GaAs since GaAs has acceptors and GaAs conduction band is empty. Afterward, electrons gather near the interface between GaAs and AlGaAs because of attraction by positive donors in AlGaAs. Finaly, electrons in AlGaAs are prevented from moving to the GaAs by the repulsion of electrons in GaAs and attraction of positive donors. This dipole layer formed from positive donors and the electrons gives rise to a potential discontinuity which finally makes the Fermi level of the GaAs equal to that of the AlGaAs. Therefore the two-dimensional electron system is formed near the interface between GaAs and AlGaAs at low temperature. Fig.1.1-(a) shows the band structure in the GaAs-AlGaAs heterostructure which has no donor. Fig.1.1-(b) shows the band structure GaAs-AlGaAs heterostructure in which AlGaAs is doped.

In GaAs with high mobility, the two-dimensional electron system can be regarded as the free electron system. Schrodinger equation in the two-dimensional free electron system in which a magnetic field is applied perpendicular to the layer of 2DES can be solved analyticaly. This 2DES has discrete energy levels (Landau levels) separated by the cyclotron energy. In a homogeneous system, as shown in Fig.1.2-(a), each level has a macroscopic degeneracy that is propotional to the area of the system. In real materials, scatterings broaden each of levels into a band of states which is called Landau band (see Fig.1.2-(b)). The states of electrons are localized in space expect a state at the center of each Landau band, which is called the extended state.

The 2DES in a high magnetic field perpendicular to the layer of 2DES at low temperatures is called quantum Hall system(QHS).

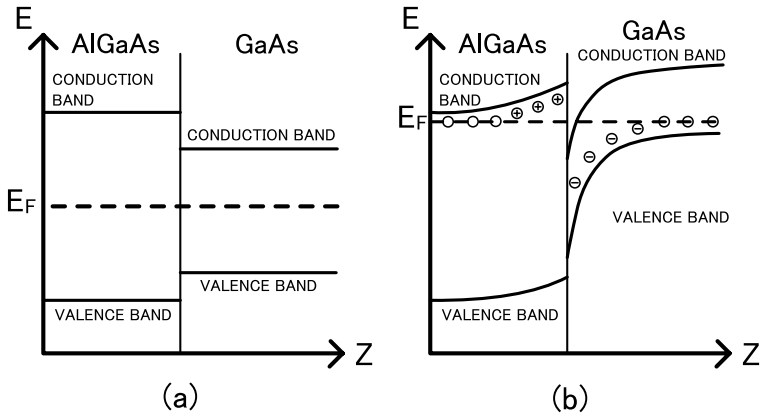

Figure 1.1: Electron energy level diagram of a GaAs-AlGaAs heterostructure device :(a) Not doping (b) Doping in AlGaAs

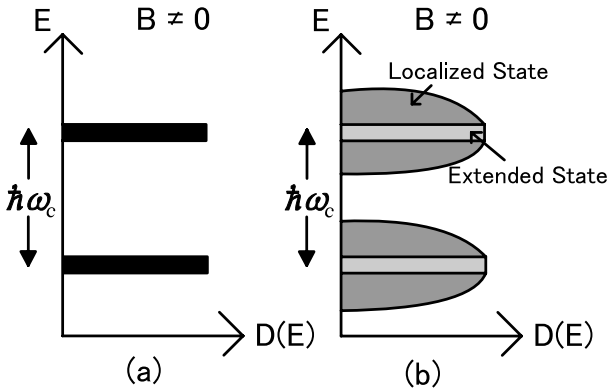

Figure 1.2: Density of states $D(E)$ vs. energy E for a two-dimensional electron gas in a magnetic field B: (a) Landau levels in a homogeneous system, and (b) Landau band in a disordered system. $\hbar\omega_c$ is the cyclotron energy, and l_c is the magnetic length.

1.1.3 Integer Quantum Hall Effect

The Hall effect was discovered by E. H. Hall in 1879. If a current perpendicular to a magnetic field flows in a sample, the electric field perpendicular to the current and the magnetic field is generated. This is called the Hall effect. The mechanism of this effect is as follows. Charged particles in motion in a magnetic field feels a Lorentz force perpendicular to their direction of the motion and the magnetic field. These charged particles accumulate to one side of the sample by the Lorentz force as shown in Fig.1.3. Thereafter the equilibrium is achieved when the magnetic force is balanced by the electrostatic force from the build up of charge at the edge. This electrostatic force is called the Hall electric field. The voltage drop at right angles to the current is called the Hall voltage. This Hall voltage increases in proportion to the strength of the magnetic field.

Investigating the Hall electric field in the system, we can know the kind of carriers and the density of carriers in the system since the formula of the Hall resistance contains the charge of carriers and the density of carriers.

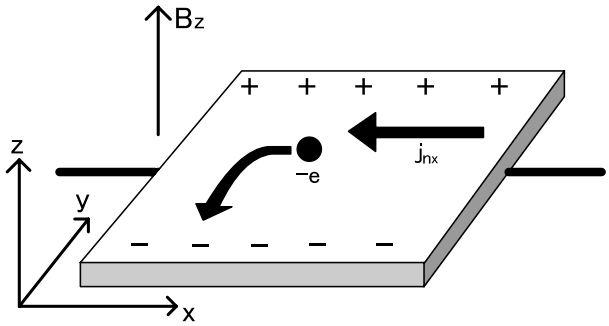

Figure 1.3: Classical Hall effect. j_{nx} is the number flux of electrons.

The integer quantum Hall effect(IQHE) was discovered by K. von Klitzing and others in 2DES in 1980. In the sample in a high magnetic field at low temperature, they found the quantization of the Hall resistance written as $R_H = h/ie^2$: Planck's constant h and the electron charge e.

The typical measurement of the Hall resistance in 2DES is as follows. Fig.1.4 shows the experimental setup. Electrons pass from a source contact S to a drain contact D along a sample. A current I flows in the sample of the geometry which is known as a Hall bar. The measured quantities are the current, the longitudinal voltage difference V_L between contacts A and B, and the transverse voltage (Hall voltage) V_H between contacts A and C.

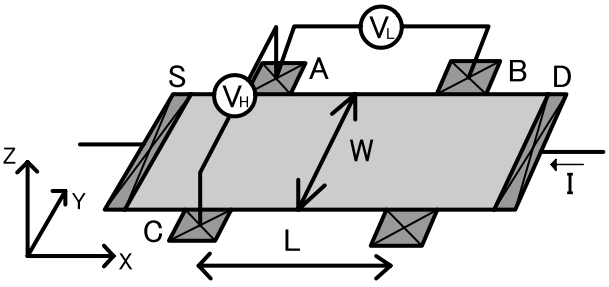

Figure 1.4: Schemaic view of a rectangular Hall bar for measurements of the quantum Hall effect. There is a two dimensional electron gas(2DEG) between a source contact S and drain contact D. The magnetic field is in the z-direction perpendicular to the plane of the 2DEG.

A typical experimental result is shown in Fig.1.5. The Hall resistance R_{xy} and the diagonal

resistivity ρ_{xx} are shown as a function of magnetic field B. R_{xy} and ρ_{xx} are obtained by using the relations $R_{xy} = V_H/I$ and $\rho_{xx} = V_x W/IL$. In the 2DES in a high magnetic field at low temperature, the Hall resistance is not simply proportional to the strength of the magnetic field. It increases in quantized steps which is called plateau. At the center of each step, the diagonal resistivity falls to zero accurately. Where the diagonal resistivity is zero, two-dimensional electrons carry current with no energy dissipation, much like a superconductor does. This discovery of IQHE is a remarkable achievement in condensed matter physics. K. von Klitzing won the Nobel Prize in physics in 1985.

Since the accuracy of this quantization was found to be better than 1 ppm, the quantization of the Hall resistance is used as the standard of resistance since 1990.

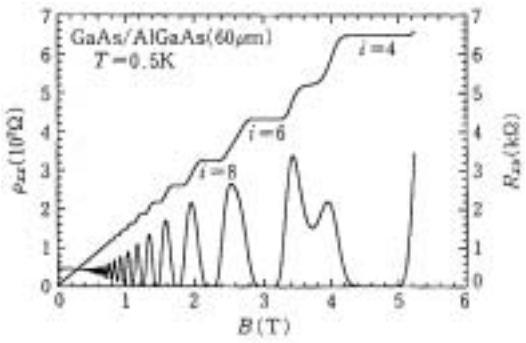

Figure 1.5: Measured diagonal resitivity ρ_{xx} and Hall resistance R_{xy} as a function of the magnetic field in a GaAs/AlGaAs heterostructure.[Okuno, Oorui, Okamoto, Kawaji, Sakai and Kurata]

1.1.4 Breakdown of the Integer Quantum Hall Effect

When we use the IQHE as the standard of resistance, we make a current large so that the Hall resistance is measured with high precision. However, increasing the current, ρ_{xx} suddenly rises many orders of magnitude within a narrow range of the current at a certain current, which is called a critical curernt as shown in Fig.1.6. Above the critical current, the nondissipative current flow breaks down . This physical limits of the IQHE is called the breakdown phenomenon of the IQHE. Up to the present, various theoretical works on mechanisms to explain experimental results of the breakdown have been reported.[1, 2, 3, 4, 5, 6, 8]

The mechanism of the breakdown has not been fully understood however. One of the explanation for the origin of the breakdown is the super-heating of the electron system. In this hot-electron model, we assume that the change of the diagonal conductivity is described by the change of the electron temperature $T_{\rm e}$. Their hot-electron model provided excellent fits to the data in the experiment by S. Komiyama et al.[3].

1.1.5 Experiment on the Spatial Variation of the Temperature in 2DES with the Gate Electrode

An interesting experiment in QHS were made by U.Klass et al.[14] in 1991. In their experiments, they measured spatial variations of temperature in the Hall bar , which is partly covered by the gate electrode. The result is shown in Fig.1.7. The temperature becomes high in the corners of the region covered by the gate electrode. I call this corner a hot spot. The filling factor changes at the neighborhood of the boundary between the region covered by the gate electrode and the region which is not covered. This rise of the temperature is similar to the rise of the temperature in two opposite corners (called hot-spot) near the current contacts.

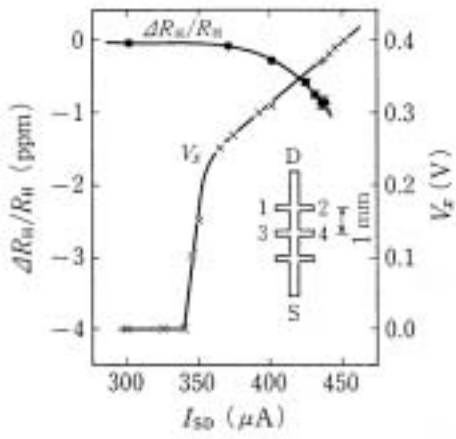

Figure 1.6: Current dependence of $\Delta R_H/R_H \equiv R_H(I_{SD})/R_H(25\mu A) - 1$ and V_x over the critical current region of a GaAs heterostructure device at 1.1K. Also shown are the source, drain, and four potential probes. M. E. Cage et al.(1983)[13].

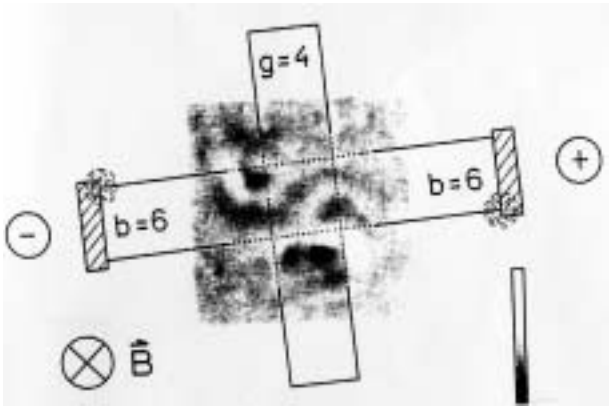

Figure 1.7: Photograph of the dissipation in the gated regions. The sample structure is indicated by the black lines.[14]

1.2 Thermohydrodynamics in Quantum Hall Systems

Akera et al.[7, 8, 19] developed a theory of thermohydrodynamics in QHS. They described spatio-temporal variations of the electron temperature and the chemical potential in the local equilibrium including the nonlinear transport regime with use of the equations of conservation. There are some theoretical calculations by using their theory.

1.2.1 Ettingshausen Effect

One of the theoretical calculations by the theory of thermohydrodynamics in QHS is the electron temperature distribution perpendicular to a current. K. Shimoyama[16] showed that the Ettingshausen effect occurs in the system, in which the potential in equilibrium has no dependence on x (along the current) and increases to an unlimited extent in the edge of the sample. In the Ettingshausen effect, the gradient of the electron temperature is developed in the direction perpendicular to the current in the presence of the magnetic field. Shimoyama shows that the gradient of the electron temperature has the variation as a function of the filling factor in the Ettingshausen effect in the QHS. In general, the sign of the gradient of the electron temperature depends on the direction of the current and that of the magnetic field. In the QHS, the sign of the gradient of the electron temperature also depends on the filling factor. Therefore we anticipate that the spatial variations of the filling factor causes interesting variations of the electron temperature in the QHS. T. Maeda[18] investigated how the spatial variations of the filling factor influence the distribution of the electron temperature in the system, in which the potential in equilibrium has no dependence on x and is smoothly varying in the y direction. He showed the potential variation is important for the spatial variation of the electron temperature.

1.2.2 Theoretical Calculation on the Spatial Variation of the Electron Temperature in 2DES with Potential Steps

T. Nakagawa[17] investigated how the potential variations parallel to the current influence the distribution of the electron temperature in QHS. He employed a model potential which changes discontinuously at the boundary between the different regions. The result is shown in Fig.1.8. The result shows that the electron temperature rises near the boundary ($x = L_x$), and the gradient of the electron temperature near a hot spot is larger. The result has something in common with that of the experiment by U.Klass et al.. He couldn't however discuss the variation of the electron temperature near this boundary quantitatively since the electron temperature distribution is not convergent with the number of calculation points employed in the difference equations. Therefore he couldn't compare the electron temperature distribution with that of the experiment by U. Klass et al..

1.3 Purpose of the Present Thesis

In the experiment on the spatial variation of the temperature in the system which has potential steps parallel to the current, U. Klass et al.[14] have shown that the temperature rises near the hot spot (see Fig.1.7). However, details of the temperature distribution near the hot spot have not been clarified yet because of the limited resolving power in the experiment. Then Nakagawa has investigated this system by the theoretical calculation [17]. However, details of the two-dimensional electron temperature distribution have not been clarified yet because the electron temperature distribution is not convergent with the number of calculation points employed in the difference equations. Therefore details of the electron temperature distribution near the hot spot have not been clarified yet. The purpose of this thesis is to investigate the two-dimensional electron temperature distribution near the hot spot by employing a model potential which changes smoothly in the direction parallel to the current. We

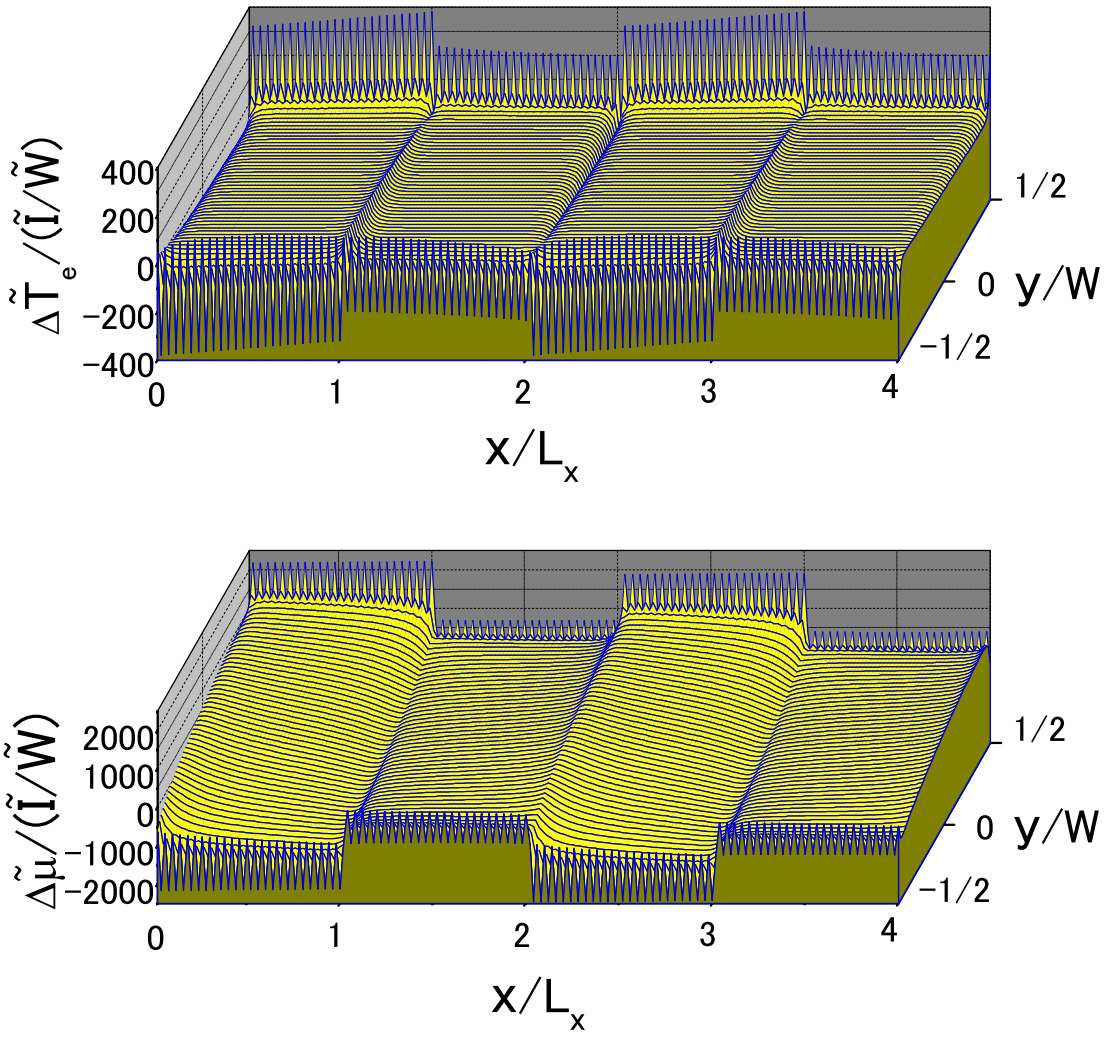

Figure 1.8: Numerical calculations of the spatial variations of the electron temperature and the electrochemical potential in the system with potential steps by T. Nakagawa[17] in the following parameters : $\tilde{W} = 1.0 \times 10^4$, the electrochemical potential in equilibrium $\tilde{\mu_{\rm ec}^{\rm eq}} = 2.25$, the potential difference $d\tilde{V} = 0.5$ and $\tilde{L_x} = 1.0 \times 10^4$. The chemical potential $\tilde{\mu}$ is $\tilde{\mu}_A = 1.75$ in the regions ($0 < x/L_x < 1$ and $2 < x/L_x < 3$) and $\tilde{\mu}_B = 2.25$ in other regions.

also investigate how the electron temperature distribution depends on various physical variables. In particular, we investigate the width dependence of the electron temperature distribution near the hot spot.

The organization of the thesis is as follows, In chapter 2, I introduce a model, processes and curernt. In chapter 3, I introduce the thermohydrodynamic equations to calculate the variation of the electron temperature and the electrochemical potential. In chapter 4, I introduce model and method for QHS with potential steps. In chapter 5, by analytical and numerical calculations, I investigate the spatial variation of the electron temperature and the electrochemical potential in the Hall bar in which the equilibrium potential has no dependence on x. In chapter 6, I calculate the spatial variation of the electron temperature and the electrochemical potential in the Hall bar, which has potential steps. In chapter 7, summary is given.

Chapter 2

Model, Processes and Current

2.1 Drift and Hopping processes

The number flux density $\boldsymbol{j}_n$ is produced by transitions of electrons. I consider two types of transitions in this thesis: drift and hopping processes.

Drift process is the motion that electron drifts along the equipotential line. The number flux density by drift process is denoted as $\boldsymbol{j}_n^{\text{drift}}$. The number flux density by drift process in discontinuous potential are denoted as $\boldsymbol{j}_n^{\text{edge}}$.

Hopping process is the motion that a localized wave packet of electron hops in intra-Landau level by a scattering from other electrons. The number flux density by this process are called $\boldsymbol{j}_n^{\text{hop}}$.

Therefore,the total number flux density $\boldsymbol{j}_n$is

$$\boldsymbol{j}_n = \boldsymbol{j}_n^{\text{drift}} + \boldsymbol{j}_n^{\text{hop}}. \tag{2.1}$$

If electrons move,they produce the thermal flux density $\boldsymbol{j}_q$. I call them $\boldsymbol{j}_q^{\text{edge}}$, $\boldsymbol{j}_q^{\text{drift}}$,$\boldsymbol{j}_q^{\text{hop}}$ in the same way I call the number flux density.

2.2 Drift current

The local flux density due to drift motion fluctuates spatially because the local potential V_{loc} contains the random potential. To obtain the macroscopic flux density, I avarage the local flux density. If the potential fluctuation length scale l_{loc} is much larger than the magnetic length $l = \sqrt{\hbar c/e|B|}(e > 0)$ which is about 0.01 μm at $|B| = 5\text{T}$, the macroscopic number flux density in the Landau level N, $\boldsymbol{j}_{nN}^{\text{drift}}$, written as

$$\boldsymbol{j}_{nN}^{\text{drift}} = \left\langle f(\varepsilon_N^0 + V_{\text{loc}}, \mu_{\text{ec}}, T_{\text{e}}) h^{-1} s_B \hat{\epsilon} \nabla V_{\text{loc}} \right\rangle_{\text{av}}, \tag{2.2}$$

with

$$s_B = \frac{B}{|B|}, \hat{\epsilon} = \begin{pmatrix} 0 & 1 \\ -1 & 0 \end{pmatrix}, \tag{2.3}$$

$$f(\varepsilon, \mu_{\text{ec}}, T_{\text{e}}) = \frac{1}{1 + \exp(\frac{\varepsilon - \mu_{\text{ec}}}{k_B T_{\text{e}}})}. \tag{2.4}$$

Since localized states make no contributions to the macroscopic flux density, the occupation probability of localized states in the above equation can be replaced by that of extended states.Then I have

$$\boldsymbol{j}_{nN}^{\text{drift}} = f(\varepsilon_N^0 + V, \mu_{\text{ec}}, T_{\text{e}}) \left\langle h^{-1} s_B \hat{\epsilon} \boldsymbol{\nabla} V_{\text{loc}} \right\rangle_{\text{av}}. \tag{2.5}$$

Since the spatial average of $\boldsymbol{\nabla} V_{\rm loc}$ is equal to $\boldsymbol{\nabla} V$(Fig.2.1),then the number flux density $\boldsymbol{j}_n^{\rm drift}$ due to all the Landau levels becomes

$$\boldsymbol{j}_n^{\rm drift} = L_{yx}^{11} \hat{\epsilon} \boldsymbol{\nabla} V, \tag{2.6}$$

with

$$L_{yx}^{11} = \frac{\sigma_{yx}}{e^2} = 2\frac{s_B}{h} \sum_{N=0}^{\infty} f_N. \tag{2.7}$$

Here I assume that the spin splitting is neglected. I call L_{yx}^{11} a transport coefficient. Similarly, I have for the thermal flux density

$$\boldsymbol{j}_q^{\rm drift} = K_{yx}^{21} \hat{\epsilon} \boldsymbol{\nabla} V, \tag{2.8}$$

with

$$K_{yx}^{21} = 2\frac{s_B}{h} \sum_{N=0}^{\infty} (\varepsilon_N^0 + V - \mu_{\rm ec}) f_N. \tag{2.9}$$

This expresses that an electron in the Landau level N carries a thermal energy $\varepsilon_N^0 + V - \mu_{\rm ec}$.

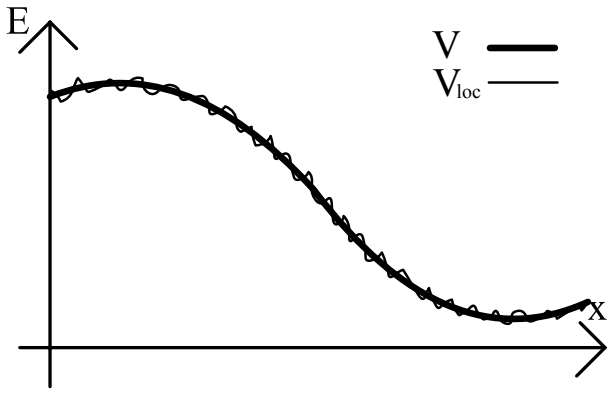

Figure 2.1: Schematic drawing of the local potential $V_{\rm loc}$ and the macroscopic potential V.

2.3 Hopping current

I assume that the number and thermal flux density by hopping process is given as

$$\boldsymbol{j}_n^{\rm hop} = -2\sum_{n=0}^{\infty} D_n \left(\frac{\partial f_n}{\partial \mu_{\rm ec}} \boldsymbol{\nabla} \mu_{\rm ec} + \frac{\partial f_n}{\partial T_{\rm e}} \boldsymbol{\nabla} T_{\rm e} \right), \tag{2.10}$$

$$\boldsymbol{j}_q^{\rm hop} = -2\sum_{n=0}^{\infty} D_n (\varepsilon_n^0 - \mu) \left(\frac{\partial f_n}{\partial \mu_{\rm ec}} \boldsymbol{\nabla} \mu_{\rm ec} + \frac{\partial f_n}{\partial T_{\rm e}} \boldsymbol{\nabla} T_{\rm e} \right). \tag{2.11}$$

Here the chemical potential $\mu(\boldsymbol{r}, t)$ is defined by $\mu = \mu_{\rm ec} - V$ and D_n is written in terms of transition rate of each hopping process, which depends on the disorder potential. The disorder potential is a function of μ and $T_{\rm e}$. I assume the N dependence of D_n to be $D_n = (2N+1)D_0$ with D_0 the coefficient for $N = 0$. These assumptions are pertinent in the macroscopic scale.

I write $\boldsymbol{j}_n^{\rm hop}$ as

$$\boldsymbol{j}_n^{\rm hop} = -L_{xx}^{11} \boldsymbol{\nabla} \mu_{\rm ec} - L_{xx}^{12} T_{\rm e}^{-1} \boldsymbol{\nabla} T_{\rm e}. \tag{2.12}$$

From eq.(2.11) I have

$$L_{xx}^{11} = e^{-2}\sigma_{xx} = (k_{\rm B}T_{\rm e})^{-1} \sum_{n=0}^{\infty} D_n f_n (1 - f_n), \tag{2.13}$$

$$L_{xx}^{12} = (k_{\rm B}T_{\rm e})^{-1}\sum_{n=0}^{\infty} D_n f_n(1-f_n)(\varepsilon_n^0-\mu). \tag{2.14}$$

Similarly, I have thermal flux density

$$\boldsymbol{j}_q^{\rm hop} = -L_{xx}^{21}\boldsymbol{\nabla}\mu_{\rm ec} - L_{xx}^{22}T_{\rm e}^{-1}\boldsymbol{\nabla}T_{\rm e}. \tag{2.15}$$

with

$$L_{xx}^{21} = L_{xx}^{12}, \tag{2.16}$$

$$L_{xx}^{22} = (k_{\rm B}T_{\rm e})^{-1}\sum_{n=0}^{\infty} D_n f_n(1-f_n)(\varepsilon_n^0-\mu)^2. \tag{2.17}$$

2.4 Edge current

The fluxes in the edge region in which the potential increases to an unlimited extent is the drift fluxes. I introduce coordinates (ξ,η) for each boundary of the two-dimensional system. The unit vector normal to the boundary, directed to the outside of the sample, is denoted by $\boldsymbol{n}$. I take the η axis in the direction of $\boldsymbol{n}$ and the ξ axis along the boundary in the direction of $\hat{\epsilon}\boldsymbol{n}$. In the region $\eta_{\rm edge} < \eta < \eta_{\rm edge}+\Delta\eta$, the drift flux $\boldsymbol{J}_n^{\rm edge}$ is written as

$$\boldsymbol{J}_n^{\rm edge} = \int_{\eta_{\rm edge}}^{\eta_{\rm edge}+\Delta\eta} \boldsymbol{j}_n^{\rm drift} d\eta. \tag{2.18}$$

Therefore, I have

$$\boldsymbol{J}_n^{\rm edge} = K_n\hat{\epsilon}\boldsymbol{n}, \tag{2.19}$$

with

$$K_n = 2\frac{s_{\rm B}}{h}\sum_{n=0}^{\infty}\int_{\eta_{\rm edge}}^{\eta_{\rm edge}+\Delta\eta} d\eta\frac{\partial V}{\partial\eta}f(\varepsilon_n^0+V,\mu_{\rm ec},T_{\rm e}). \tag{2.20}$$

Since the η dependence of $\mu_{\rm ec}$ and $T_{\rm e}$ is neglected,

$$K_n = 2\frac{s_{\rm B}}{h}\sum_{n=0}^{\infty}\int_{\varepsilon_n}^{\infty} f(\varepsilon,\mu_{\rm ec},T_{\rm e})d\varepsilon \tag{2.21}$$

where ε_n,$\mu_{\rm ec}$ and $T_{\rm e}$ are to be evaluated at $\eta_{\rm edge}$. The quantity K_n is related to the magnetization per unit area, M, at $\eta_{\rm edge}$ by

$$K_n(\eta_{\rm edge}) = (c/e)M(\eta_{\rm edge}), \tag{2.22}$$

since the edge electric current $\boldsymbol{I}$ and M are related by $\boldsymbol{I} = -cM\hat{\epsilon}\boldsymbol{n}$. The thermal flux is given by

$$\boldsymbol{J}_q^{\rm edge} = K_q\hat{\epsilon}\boldsymbol{n}, \tag{2.23}$$

with

$$K_q = 2\frac{s_{\rm B}}{h}\sum_{n=0}^{\infty}\int_{\varepsilon_n}^{\infty}(\varepsilon-\mu_{\rm ec})f(\varepsilon,\mu_{\rm ec},T_{\rm e})d\varepsilon. \tag{2.24}$$

2.5 Transport current

These fluxes are produced not only by $\boldsymbol{\nabla}\mu_{\rm ec}$ and $\boldsymbol{\nabla}T_{\rm e}$, but also by $\boldsymbol{\nabla}V$, and therefore they are in general nonzero in equilibrium. The standard transport experiment measures a flux through a cross section of the sample, which is zero in equilibrium. I introduce such a flux $\boldsymbol{j}_n^{\rm tr}$, which is induced in nonequilibrium. Subtracting the magnetization current which is nonzero in equilibrium, I obtaine the transport fluxes:

$$\boldsymbol{j}_n^{\rm tr} = \boldsymbol{j}_n - \hat{\epsilon}\boldsymbol{\nabla}M_n,\ \boldsymbol{j}_\varepsilon^{\rm tr} = \boldsymbol{j}_\varepsilon - \hat{\epsilon}\boldsymbol{\nabla}M_\varepsilon, \tag{2.25}$$

with

$$M_n = K_n,\ M_\varepsilon = -(K_q + \mu_{\rm ec}K_n), \tag{2.26}$$

$$j_{nx}(\boldsymbol{r},t) = -L_{xx}^{11}\nabla_x\mu_{\rm ec} + L_{yx}^{11}\nabla_y V - \frac{L_{xx}^{12}}{T_{\rm e}}\nabla_x T_{\rm e}, \tag{2.27}$$

$$j_{ny}(\boldsymbol{r},t) = -L_{yx}^{11}\nabla_x V - L_{xx}^{11}\nabla_y\mu_{\rm ec} - \frac{L_{xx}^{12}}{T_{\rm e}}\nabla_y T_{\rm e}, \tag{2.28}$$

$$j_{qx}(\boldsymbol{r},t) = -L_{xx}^{21}\nabla_x\mu_{\rm ec} + K_{yx}^{21}\nabla_y V - \frac{L_{xx}^{22}}{T_{\rm e}}\nabla_x T_{\rm e}, \tag{2.29}$$

$$j_{qy}(\boldsymbol{r},t) = -K_{yx}^{21}\nabla_x V - L_{xx}^{21}\nabla_y\mu_{\rm ec} - \frac{L_{xx}^{22}}{T_{\rm e}}\nabla_y T_{\rm e}, \tag{2.30}$$

where $\boldsymbol{j}_\varepsilon^{\rm tr}$ and $\boldsymbol{j}_q^{\rm tr}$ are related by $\boldsymbol{j}_q^{\rm tr} = \boldsymbol{j}_\varepsilon^{\rm tr} - \mu_{\rm ec}\boldsymbol{j}_n^{\rm tr}$, and K_n and K_q are now to be evaluated at a point $\boldsymbol{r}$ within the sample.

Therefore, the transport flux densities are difined at each point $\boldsymbol{r}$ by

$$j_{nx}^{\rm tr}(\boldsymbol{r},t) = -L_{xx}^{11}\nabla_x\mu_{\rm ec} + L_{yx}^{11}\nabla_y\mu_{\rm ec} - \frac{L_{xx}^{12}}{T_{\rm e}}\nabla_x T_{\rm e} + \frac{L_{yx}^{12}}{T_{\rm e}}\nabla_y T_{\rm e}, \tag{2.31}$$

$$j_{ny}^{\rm tr}(\boldsymbol{r},t) = -L_{yx}^{11}\nabla_x\mu_{\rm ec} - L_{xx}^{11}\nabla_y\mu_{\rm ec} - \frac{L_{yx}^{12}}{T_{\rm e}}\nabla_x T_{\rm e} - \frac{L_{xx}^{12}}{T_{\rm e}}\nabla_y T_{\rm e}, \tag{2.32}$$

$$j_{qx}^{\rm tr}(\boldsymbol{r},t) = -L_{xx}^{21}\nabla_x\mu_{\rm ec} + L_{yx}^{21}\nabla_y\mu_{\rm ec} - \frac{L_{xx}^{22}}{T_{\rm e}}\nabla_x T_{\rm e} + \frac{L_{yx}^{22}}{T_{\rm e}}\nabla_y T_{\rm e}, \tag{2.33}$$

$$j_{qy}^{\rm tr}(\boldsymbol{r},t) = -L_{yx}^{21}\nabla_x\mu_{\rm ec} - L_{xx}^{21}\nabla_y\mu_{\rm ec} - \frac{L_{yx}^{22}}{T_{\rm e}}\nabla_x T_{\rm e} - \frac{L_{xx}^{22}}{T_{\rm e}}\nabla_y T_{\rm e}, \tag{2.34}$$

with

$$L_{yx}^{12} = T_{\rm e}\frac{\partial K_n}{\partial T_{\rm e}}, \tag{2.35}$$

$$L_{yx}^{21} = L_{yx}^{12}, \tag{2.36}$$

$$L_{yx}^{22} = T_{\rm e}\frac{\partial K_q}{\partial T_{\rm e}}. \tag{2.37}$$

Chapter 3

Equations of Thermohydrodynamics

3.1 Equations of conservation

There are two equations of conservation in our model of quantum Hall systems. One describes the conservation of the electron number, and the other describes the conservation of the energy. The equation of the electron number conservation is

$$\frac{\partial n}{\partial t} = -\boldsymbol{\nabla} \cdot \boldsymbol{j}_n, \tag{3.1}$$

where n is the electron density. The equation of the energy conservation is

$$\frac{\partial \varepsilon}{\partial t} = -\boldsymbol{\nabla} \cdot \boldsymbol{j}_\varepsilon - P_{\rm L}. \tag{3.2}$$

Here $\boldsymbol{j}_\varepsilon = \varepsilon_{local}\boldsymbol{j}_n$ is the energy flux density and ε_{local} is the energy of the electrons at a local point, while $P_{\rm L}$ is the energy loss per unit area at point $\boldsymbol{r}$ due to the heat transfer between electrons and phonons and is in general a function of μ,$T_{\rm e}$, and $T_{\rm L}$. The energy density is sum of the kinetic energy density and the potential energy density : $\varepsilon = \varepsilon_{\rm kin} + nV$.

Equations describing the time evolution of μ and $T_{\rm e}$ are derived from those of $n(\mu, T_{\rm e})$ and the entropy density $s(\mu, T_{\rm e})$, respectively. The equation for the time evolution of s is derived using eqs.(3.1),(3.2), and

$$T_{\rm e} ds = d\varepsilon - \mu_{\rm ec} dn, \tag{3.3}$$

to be

$$T_{\rm e}\frac{\partial s}{\partial t} = -\boldsymbol{\nabla} \cdot \boldsymbol{j}_q - \boldsymbol{\nabla}\mu_{\rm ec} \cdot \boldsymbol{j}_n - P_{\rm L}, \tag{3.4}$$

where $\boldsymbol{j}_q$ is defined by

$$\boldsymbol{j}_q = \boldsymbol{j}_\varepsilon - \mu_{\rm ec}\boldsymbol{j}_n. \tag{3.5}$$

I employ the simplest model of the energy loss $P_{\rm L}$:

$$P_{\rm L} = C_{\rm p}(T_{\rm e} - T_{\rm L}), \tag{3.6}$$

where $C_{\rm p}$ is a constant.

I rewrite the equations of conservation, eqs.(3.1) and (3.4), in terms of the transport flux densities. Because the divergence of each magnetization current density in eq.(2.25) is zero, the equations can be written in terms of $\boldsymbol{j}_n^{\rm tr}$ and $\boldsymbol{j}_q^{\rm tr}$ only :

$$\frac{\partial n}{\partial t} = -\boldsymbol{\nabla} \cdot \boldsymbol{j}_n^{\rm tr}, \tag{3.7}$$

$$T_{\rm e}\frac{\partial s}{\partial t} = -\boldsymbol{\nabla} \cdot \boldsymbol{j}_q^{\rm tr} - \boldsymbol{\nabla}\mu_{\rm ec} \cdot \boldsymbol{j}_n^{\rm tr} - P_{\rm L}. \tag{3.8}$$

The term $-\boldsymbol{\nabla}\mu_{\rm ec} \cdot \boldsymbol{j}_n^{\rm tr}$ is of the second order of the current.

3.2 Coefficients

I estimate $C_{\rm p}$ and D_0. $C_{\rm p}$ and D_0 can be obtained by calculating the matrix elements of electron-electron scatterings and electron-phonon scatterings. Although, these calculations are difficult. Therefore in this thesis, I estimate $C_{\rm p}$ and D_0 by using the result of the experimentation about breakdown of the quantum Hall effect by Komiyama.

I use dimensionless variables as $\tilde{T_{\rm e}} = \frac{k_{\rm B}}{\hbar\omega_c}T_{\rm e}$, $\tilde{\mu_{\rm ec}} = \frac{1}{\hbar\omega_c}\mu_{\rm ec}$, $\tilde{P_{\rm L}} = \frac{l^2}{\hbar\omega_c}P_{\rm L}, \tilde{D_0} = \frac{1}{\omega_c}D_0$ and $\tilde{C_p} = \frac{l^2}{k_{\rm B}\omega_c}C_p$. Here, a unit of length is magnetic length l, a unit of time is ω_c^{-1} and unit of energy is $\hbar\omega_c$. ω_c is an angular frequency. I consider that the system is uniform and in steady state , the filling factor is an even integer, $T_{\rm L} = 0$ and $T_{\rm e}$ is not large. I assume that two Landau levels near $\tilde{\mu}_{\rm ec}$ only contribute to the transport coefficients. Then I estimate $\tilde{\sigma}_{xx} = C_h f(1-f)$. Eq.(2.13) becomes the equation of an energy balance which is written as

$$(\tilde{P}_{\rm G} =)\ \tilde{\sigma_{xx}}\tilde{E}^2 = \tilde{C}_{\rm p}\tilde{T}_{\rm e}\ (=\tilde{P}_{\rm L}), \tag{3.9}$$

since $\boldsymbol{\nabla}\cdot\boldsymbol{j}_q = 0$. Fig.3.1 shows how $\tilde{P}_{\rm L}$ and $\tilde{P}_{\rm G}$ depend on $\tilde{T}_{\rm e}$. Increasing $\tilde{E}$, the number of an intersection point of $\tilde{P}_{\rm L}$ and $\tilde{P}_{\rm G}$ change from one to two at a value of the electric field. Then this electric field is called the critical electric field. From the experiment, I estimate dimensionless critical erectric field as $\tilde{E}_c = 8\times10^{-3}$ and $\tilde{\sigma}_{xx} = 2\times10^{-2}$. Therefore I obtain

$$\tilde{C}_{\rm p} = 6\times10^{-6}. \tag{3.10}$$

Using $\sigma_{xx} = \tilde{T_{\rm e}}^{-1}\tilde{D}_0(2N+1)f(f-1)$, I obtain

$$\tilde{D}_0 = 0.005. \tag{3.11}$$

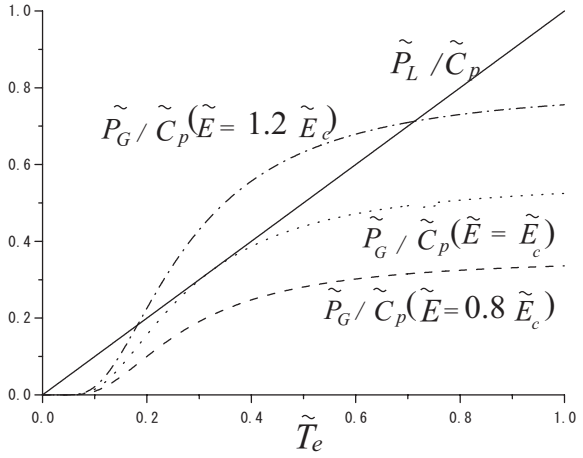

Figure 3.1: Energy-gain and Energy-loss.[6]

Chapter 4

Model and Method for Quantum Hall Systems with Potential Steps

I consider a two-dimensional system in the xy plane ($-W/2 < y < W/2$ and periodic in the x direction) in a perpendicular magnetic field $\mathbf{B} = (0, 0, B)$(see Fig.4.1). I calculate the electrochemical potential

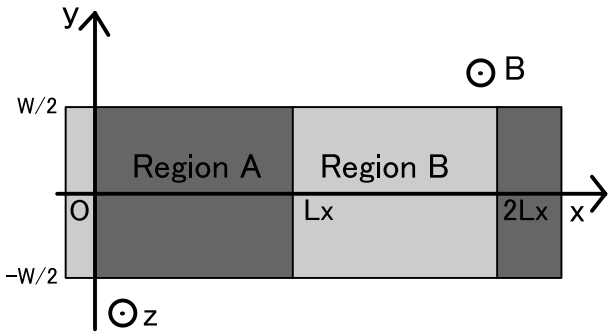

Figure 4.1: Axis of coordinates.

$\mu_{\rm ec}$ and the electron temperature $T_{\rm e}$ in steady states in this thesis.

4.1 Boundary Conditions

In this system, I use a periodic boundary condition, which is

$$\begin{aligned} T_{\rm e}(x + 2L_x, y) &= T_{\rm e}(x, y), \\ \mu_{\rm ec}(x + 2L_x, y) &= \mu_{\rm ec}(x, y) + \mu^0_{\rm ec}. \end{aligned}$$

Here $\mu^0_{\rm ec}$ is electrochemical potential difference to produce a steady current. The number flux, the thermal flux, $\mu_{\rm ec}$ and $T_{\rm e}$ are in the first order of $\mu^0_{\rm ec}$ in the linear-response regime.

In the edge of the sample, I assume that the potential increases to an unlimited extent and that electrons can't come and go between Hall bar and the outside. The boundary conditions at $y = \pm W/2$ are

$$\boldsymbol{j}^{\rm tr}_{ny} = 0,\ \boldsymbol{j}^{\rm tr}_{qy} = 0, \tag{4.1}$$

since the fluxes to the outside of the sample are absent.

4.2 Potential and Chemical Potential

If part of the Hall bar is covered by gate electrode, a potential difference (ΔV) is produced in the Hall bar(Fig.4.2). It poduces a difference in filling factor(Fig.4.3).

I consider the potential distribution which is

$$V(x) = \begin{cases} \frac{\Delta V}{1+\exp(\frac{x}{\lambda/\pi})} & (-L_x < x < L_x/2) \\ \frac{\Delta V}{1+\exp(\frac{L_x-x}{\lambda/\pi})} & (L_x/2 < x < 3/2\, L_x) \end{cases} \tag{4.2}$$

with a lengh scale λ.

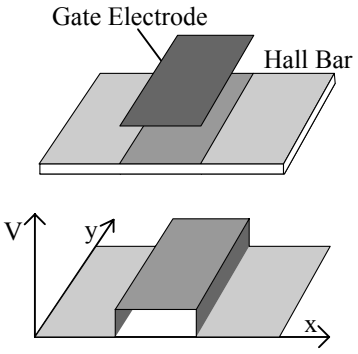

Figure 4.2: Hall bar with the gate electrode. Potential changes under the gate electrode.

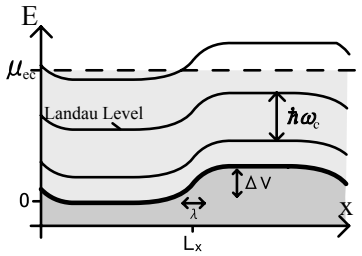

Figure 4.3: Change of the filling factor in equilibrium state.

4.3 Equations in the Linear-Response Regime

Using eqs.(3.7) and (3.8), I calculate $\mu_{\rm ec}$ and $T_{\rm e}$. However, It is difficult to solve the above equations. Therefore I restrict the calculation to the linear-response regime and to steady states. In this regime, these equations become linear partial differential equations:

$$-\boldsymbol{\nabla}\cdot\boldsymbol{j}_n^{\rm tr} = 0, \tag{4.3}$$

$$-\boldsymbol{\nabla}\cdot\boldsymbol{j}_q^{\rm tr} - P_{\rm L} = 0. \tag{4.4}$$

Using eqs.(2.31), (2.32),(2.33) and (2.34), I obtain

$$\begin{aligned} 0 &= -\frac{\partial L_{xx}^{11}}{\partial x}\nabla_x\mu_{\rm ec} + \frac{\partial L_{yx}^{11}}{\partial x}\nabla_y\mu_{\rm ec} - \frac{\frac{\partial L_{xx}^{12}}{\partial x}}{T_{\rm e}}\nabla_x T_{\rm e} + \frac{\frac{\partial L_{yx}^{12}}{\partial x}}{T_{\rm e}}\nabla_y T_{\rm e} \\ &- L_{xx}^{11}\nabla_x^2\mu_{\rm ec} - \frac{L_{xx}^{12}}{T_{\rm e}}\nabla_x^2 T_{\rm e} - L_{xx}^{11}\nabla_y^2\mu_{\rm ec} - \frac{L_{xx}^{12}}{T_{\rm e}}\nabla_y^2 T_{\rm e}, \end{aligned} \tag{4.5}$$

and

$$\begin{aligned} 0 &= -\frac{\partial L_{xx}^{21}}{\partial x}\nabla_x\mu_{\rm ec} + \frac{\partial L_{yx}^{21}}{\partial x}\nabla_y\mu_{\rm ec} - \frac{\frac{\partial L_{xx}^{22}}{\partial x}}{T_{\rm e}}\nabla_x T_{\rm e} + \frac{\frac{\partial L_{yx}^{22}}{\partial x}}{T_{\rm e}}\nabla_y T_{\rm e} \\ &- L_{xx}^{21}\nabla_x^2\mu_{\rm ec} - \frac{L_{xx}^{22}}{T_{\rm e}}\nabla_x^2 T_{\rm e} - L_{xx}^{21}\nabla_y^2\mu_{\rm ec} - \frac{L_{xx}^{22}}{T_{\rm e}}\nabla_y^2 T_{\rm e} + C_{\rm p}(T_{\rm e}-T_{\rm L}) \end{aligned} \tag{4.6}$$

with $C_{\rm p}(T_{\rm e}-T_{\rm L}) = P_{\rm L}$. The transport coefficients are to be evaluated in equilibrium since the above equations, $\boldsymbol{\nabla}\mu_{\rm ec}$ and $\boldsymbol{\nabla}T_{\rm e}$ are of the first order of the current. In the next section, I discretize the above equations and boundary conditions.

4.4 Method of the Numerical Calculation

Differential equations are transformed into difference equations. I divide the system into $2n \times n$ sites as shown in Fig.4.4. I consider the equations on each sites.

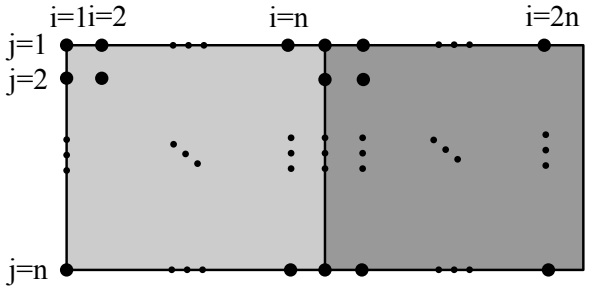

Figure 4.4: System is divided into $2n \times n$ sites.

Using the Taylar expansion, I have

$$\mu_{\rm ec}(i+1,j) = \mu_{\rm ec}(i,j) + \nabla_x \mu_{\rm ec}(i,j)\Delta x + \frac{1}{2}\nabla_x^2 \mu_{\rm ec}(i,j)(\Delta x)^2 + \cdots, \tag{4.7}$$

$$\mu_{\rm ec}(i-1,j) = \mu_{\rm ec}(i,j) - \nabla_x \mu_{\rm ec}(i,j)\Delta x + \frac{1}{2}\nabla_x^2 \mu_{\rm ec}(i,j)(\Delta x)^2 + \cdots, \tag{4.8}$$

$$\mu_{\rm ec}(i,j+1) = \mu_{\rm ec}(i,j) - \nabla_y \mu_{\rm ec}(i,j)\Delta y + \frac{1}{2}\nabla_y^2 \mu_{\rm ec}(i,j)(\Delta y)^2 + \cdots, \tag{4.9}$$

$$\mu_{\rm ec}(i,j-1) = \mu_{\rm ec}(i,j) + \nabla_y \mu_{\rm ec}(i,j)\Delta y + \frac{1}{2}\nabla_y^2 \mu_{\rm ec}(i,j)(\Delta y)^2 + \cdots. \tag{4.10}$$

From the adove expansion, I approximate $\nabla_x \mu_{\rm ec}(i,j)$,$\nabla_x^2 \mu_{\rm ec}(i,j)$, $\nabla_y \mu_{\rm ec}(i,j)$ and $\nabla_y^2 \mu_{\rm ec}(i,j)$ in the second order of Δx or Δy. I obtain

$$\frac{\partial \mu_{\rm ec}}{\partial x} \sim \frac{\mu_{\rm ec}(i+1,j) - \mu_{\rm ec}(i-1,j)}{2L_x/n}, \tag{4.11}$$

$$\frac{\partial \mu_{\rm ec}}{\partial y} \sim \frac{\mu_{\rm ec}(i,j-1) - \mu_{\rm ec}(i,j+1)}{2W/(n-1)}, \tag{4.12}$$

$$\frac{\partial^2 \mu_{\rm ec}}{\partial x^2} \sim \frac{\mu_{\rm ec}(i+1,j) - 2\mu_{\rm ec}(i,j) + \mu_{\rm ec}(i-1,j)}{(L_x/n)^2}, \tag{4.13}$$

$$\frac{\partial^2 \mu_{\rm ec}}{\partial y^2} \sim \frac{\mu_{\rm ec}(i,j-1) - 2\mu_{\rm ec}(i,j) + \mu_{\rm ec}(i,j+1)}{(W/(n-1))^2}. \tag{4.14}$$

The differential of $T_{\rm e}$ can be obtained, similarly. At the each edge($j = 1$ and $j = n$), different approximations of differential of y are needed since the adove equations can't be used without neighboring sites. Here I use the Taylar expantion:

$$\mu_{\rm ec}(i,2) = \mu_{\rm ec}(i,1) - \nabla_y \mu_{\rm ec}(i,1)\Delta y + \frac{1}{2}\nabla_y^2 \mu_{\rm ec}(i,1)(-\Delta y)^2 + \cdots, \tag{4.15}$$

$$\mu_{\rm ec}(i,3) = \mu_{\rm ec}(i,1) + \nabla_y \mu_{\rm ec}(i,1)(-2\Delta y) + \frac{1}{2}\nabla_y^2 \mu_{\rm ec}(i,1)(-2\Delta y)^2 + \cdots, \tag{4.16}$$

$$\mu_{\rm ec}(i,n-1)=\mu_{\rm ec}(i,n)+\nabla_y\mu_{\rm ec}(i,n)\Delta y+\frac{1}{2}\nabla_y^2\mu_{\rm ec}(i,n)(\Delta y)^2+\cdots, \tag{4.17}$$

$$\mu_{\rm ec}(i,n-2)=\mu_{\rm ec}(i,n)+\nabla_y\mu_{\rm ec}(i,n)(2\Delta y)+\frac{1}{2}\nabla_y^2\mu_{\rm ec}(i,n)(2\Delta y)^2+\cdots. \tag{4.18}$$

Therefore the approximations in the second order of Δy are written as

$$\frac{\partial\mu_{\rm ec}(i,1)}{\partial y}\sim\frac{3\mu_{\rm ec}(i,1)-4\mu_{\rm ec}(i,2)+\mu_{\rm ec}(i,3)}{2W/(n-1)}, \tag{4.19}$$

$$\frac{\partial\mu_{\rm ec}(i,n)}{\partial y}\sim-\frac{3\mu_{\rm ec}(i,n)-4\mu_{\rm ec}(i,n-1)+\mu_{\rm ec}(i,n-2)}{2W/(n-1)}. \tag{4.20}$$

The differential of $T_{\rm e}$ can be obtained, similarly.

Using difference equations, eqs.(4.5) and (4.6) with eq.(4.1) become to $4n^2$ simultaneous equations. I solve these simultaneous equations. Since the equations and the boundary conditions only contain the differential of $\mu_{\rm ec}$, I determine a point of reference which is written as

$$\mu_{\rm ec}(i_0,j_0)=0. \tag{4.21}$$

I choose $\mu_{\rm ec}(n,n/2)$. One equation of the simultaneous equations is replaced by eq.(4.21).

Chapter 5

Quantum Hall Systems without Potential Steps

First we consider the two-dimensional system, which has no potential variation along the current. In this system, $T_{\rm e}$ and $\mu_{\rm ec}$ can be derived analytically.

5.1 Analytical Calculation

5.1.1 Model and Equations [19]

I assume that flux densities and thermodynamic quantities have no dependence on x. The exception is $\mu_{\rm ec}$ which has a constant gradient along x. The gradient $\nabla_x\mu_{\rm ec}$ is also independent of y since $\nabla_y\nabla_x\mu_{\rm ec} = \nabla_x\nabla_y\mu_{\rm ec} = 0$, and is equal to $\nabla_x V = eE_x$. Then $\nabla_x j^{\rm tr}_{nx}$ and $\nabla_x j^{\rm tr}_{qx}$ become

$$\nabla_x j^{\rm tr}_{nx} = 0, \tag{5.1}$$
$$\nabla_x j^{\rm tr}_{qx} = 0. \tag{5.2}$$

Therefore the equations of conservation are written as

$$\nabla_y j^{\rm tr}_{ny} = 0, \tag{5.3}$$
$$\nabla_y j^{\rm tr}_{qy} + C_{\rm p}(T_{\rm e} - T_{\rm L}) = 0. \tag{5.4}$$

Using eq.(5.3) and the boundary conditions at $y = \pm W/2$, I have

$$j^{\rm tr}_{ny} = 0, -W/2 < y < W/2. \tag{5.5}$$

5.1.2 Spatial Variations of the Electron Temperature [19]

I substitute $\nabla_x\mu_{\rm ec} = eE_x$ and $\nabla_x T_{\rm e} = 0$ into the formula of $j^{\rm tr}_{qy}$, and use eq.(5.5) to eliminate $\nabla_y\mu_{\rm ec}$. Then I obtain

$$j^{\rm tr}_{qy} = -A^{21}_{yx} eE_x - A^{22}_{yy}\nabla_y T_{\rm e}, \tag{5.6}$$

with

$$A^{21}_{yx} = L^{21}_{yx} - L^{21}_{yy}(L^{11}_{yy})^{-1}L^{11}_{yx}, \tag{5.7}$$
$$A^{22}_{yy} = [L^{22}_{yy} - L^{21}_{yy}(L^{11}_{yy})^{-1}L^{12}_{yy}]T_L^{-1}. \tag{5.8}$$

The transport coefficients are constant in the linear-response regime. Substituting eq.(5.6) into eq.(5.4), I obtain the equation for $T_{\rm e}$:

$$A^{22}_{yy}\nabla^2_y T_{\rm e} = C_{\rm p}(T_{\rm e} - T_{\rm L}), \tag{5.9}$$

with the boundary condition:

$$j_{qy}^{\rm tr} = -A_{yx}^{21} eE_x - A_{yy}^{22} \nabla_y T_{\rm e} = 0, y = \pm W/2. \tag{5.10}$$

This boundary condition immediately shows that the electric field E_x along the current induces the temperature gradient $\nabla_y T_{\rm e}$. Solving the equation, I find the spatial variation of $T_{\rm e}$ to be

$$T_{\rm e}(y) - T_{\rm L} = T_0[e^{-(y+W/2)/\lambda_T} - e^{(y-W/2)/\lambda_T}]. \tag{5.11}$$

The relaxation length of the $T_{\rm e}$ deviation is found to be

$$\lambda_T = (A_{yy}^{22}/C_{\rm p})^{1/2}. \tag{5.12}$$

The magnitude of the $T_{\rm e}$ deviation is

$$T_0 = (\lambda_T A_{yx}^{21}/A_{yy}^{22})(1 + e^{-W/\lambda_T})^{-1} eE_x. \tag{5.13}$$

I make a rough estimate of λ_T. Since

$$L_{yy}^{11} \sim (k_{\rm B}T_{\rm e})^{-1} D_0, \tag{5.14}$$

$$L_{yy}^{21} \sim D_0, \tag{5.15}$$

$$L_{yy}^{22} \sim D_0(k_{\rm B}T_{\rm e}), \tag{5.16}$$

$$\tag{5.17}$$

I find that

$$A_{yy}^{22} \sim k_{\rm B} D_0. \tag{5.18}$$

Using $C_p = 6.0 \times 10^{-6}$ and $D_0 = 0.005$, λ_T is estimated to be

$$\lambda_T \sim 0.01 \mu m. \tag{5.19}$$

Using eq.(5.5) and eq.(5.11), I find the spatial variation of $\mu_{\rm ec}$ to be

$$\mu_{\rm ec} = -\frac{L_{yx}^{11}}{L_{yy}^{11}} eE_x y - \frac{1}{T_{\rm L}} \frac{L_{yy}^{21}}{L_{yy}^{11}} T_{\rm e}(y) + const.. \tag{5.20}$$

The result is shown in Fig.5.6.

5.1.3 Diagonal Resistivity

I substitute $\nabla_x \mu_{\rm ec} = eE_x$ and $\nabla_x T_{\rm e} = 0$ into the formula of $j_{nx}^{\rm tr}$, and use eq.(5.5) to eliminate $\nabla_y \mu_{\rm ec}$. Then I obtain

$$j_{nx}^{\rm tr} = -A_{yy}^{11} eE_x + A_{yx}^{21} T_{\rm L}^{-1} \nabla_y T_{\rm e}, \tag{5.21}$$

with

$$A_{yy}^{11} = L_{yy}^{11} + (L_{yx}^{21})^2 (L_{yy}^{11})^{-1}. \tag{5.22}$$

The number flux$J_{nx}^{\rm tr}$ is given by

$$J_{nx}^{\rm tr} = \int_{-W/2}^{W/2} j_{nx}^{\rm tr} dy. \tag{5.23}$$

Using eq.(5.21) and eq.(5.11), I obtain

$$J_{nx}^{\rm tr} = -W A_{yy}^{11} eE_x + 2A_{yx}^{21} \frac{T_0}{T_{\rm L}} (e^{-W/\lambda_T} - 1). \tag{5.24}$$

We know that $J_{nx}^{\rm tr}$ is extremely small at each Landau level. In the region of $\lambda_T \sim W$, I obtain the result that $J_{nx}^{\rm tr}$ shows local maximum between the neighboring Landau levels(see Fig.5.1, Fig.5.2 and Fig.5.3).

$J_{nx}^{\rm tr}$ shows local maximum between the neighboring Landau levels because $J_{nx}^{\rm tr}$ is induced also by $\nabla_y T_{\rm e}$. There is the gradient of the electron temperature due to Ettingshausen effect. The gradient of $T_{\rm e}$ is larger near the edge. This variation length is λ_T. Therefore, In the region of $W \sim \lambda_T$, $J_{nx}^{\rm tr}$ is affected by the gradient of $T_{\rm e}$.

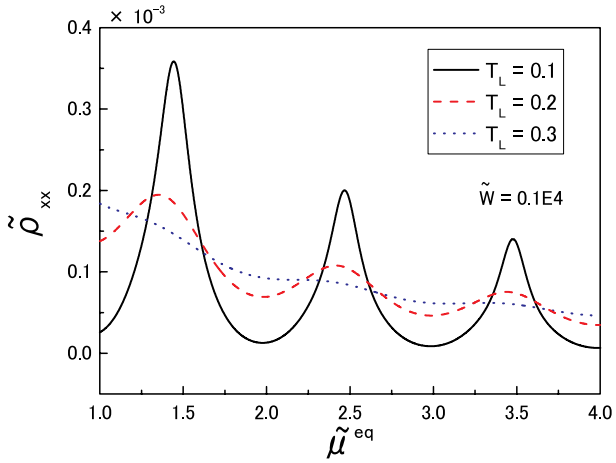

Figure 5.1: Variation of the diagonal resistivity in the following parameters: $\tilde{L_x} = 1.0 \times 10^4$ and $\tilde{W} = 0.1 \times 10^4$.

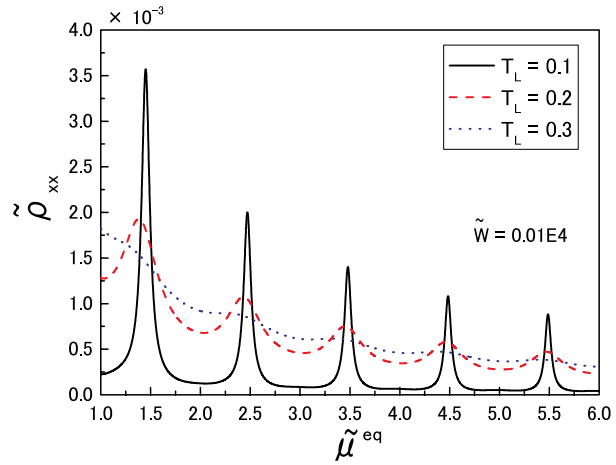

Figure 5.2: Variation of the diagonal resistivity in the following parameters: $\tilde{L_x} = 1.0 \times 10^4$ and $\tilde{W} = 0.01 \times 10^4$.

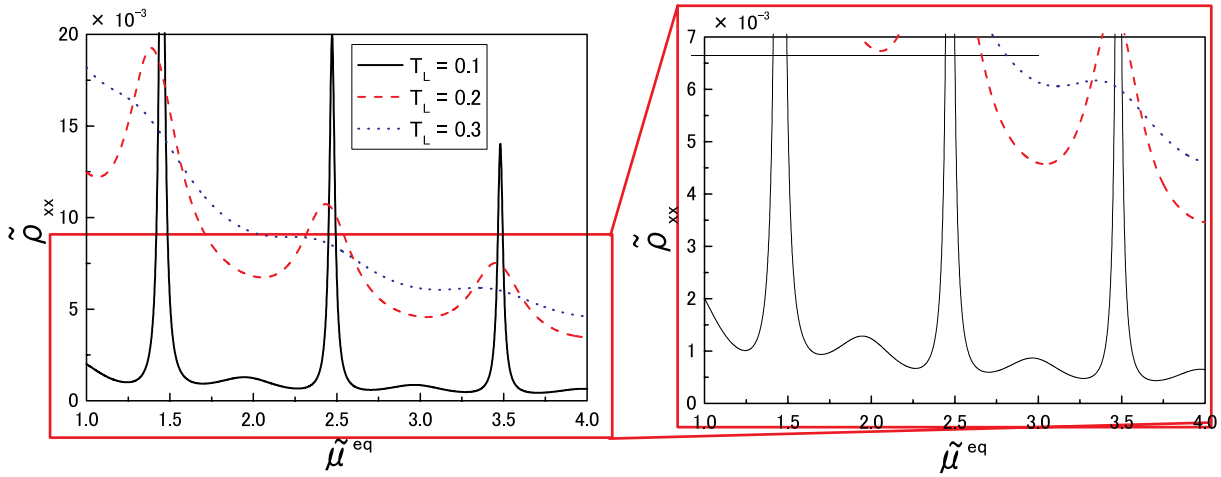

Figure 5.3: Variation of the diagonal resistivity in the following parameters: $\tilde{L_x} = 1.0 \times 10^4$ and $\tilde{W} = 0.001 \times 10^4$.

5.1.4 Quantum Oscillations of the Electron Temperature

I investigate $\mu^{\rm eq}$ dependence of the change of the electron temperature $\Delta T_{\rm e} = T_{\rm e}(W/2) - T_{\rm e}(0)$. I show in Fig.5.4. I obtain the result that the sign of $\Delta T_{\rm e}$ exhibits quantum oscillations as a function of μ. Whenever μ increase every $0.5\hbar\omega$, the sign of $\Delta T_{\rm e}$ is reversed since the kind of carriers changes(Fig.5.5)[16].

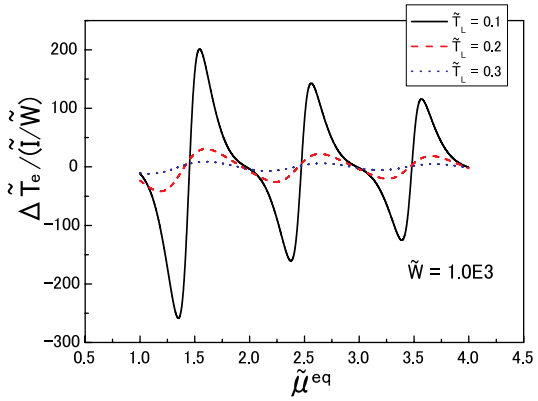

Figure 5.4: Variation of $\Delta T_{\rm e}$ in the following parameters: $\tilde{L_x} = 1.0 \times 10^4$ and $\tilde{W} = 0.1 \times 10^4$.

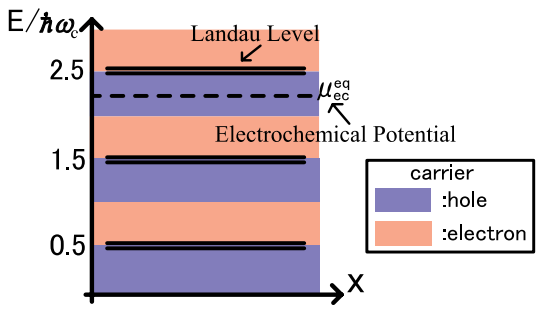

Figure 5.5: Change of filling factor in equilibrium state.

5.2 Numerical Calculation

I have investigated this system by two methods. One is an analytical calculation, and the other is a numerical calculation. I have calculated a spatial variation of the electron temperature and that of the chemical potential in the following parameters: the number of the site $N = 50$, the length of the system $\tilde{L_x} = \tilde{W} = 1 \times 10^3$ (about $10\mu m$ at $B = 5$T) , $\tilde{T_{\rm L}} = 0.1$ (about 10K at $B = 5$T) and chemical potential in equilibrium $\tilde{\mu}^{\rm eq} = 2.25$. Fig.5.6 shows the result. In the edge region, the gradient of electron temperature is large. Estimating $\Delta T_{\rm e}$ at $\tilde{I}/\tilde{W} = 0.1$, $B = 5$T, it is about 5K. IQHE can be found in this situation and the current is $0.1A/m$. These calculations by each methods are consistent.

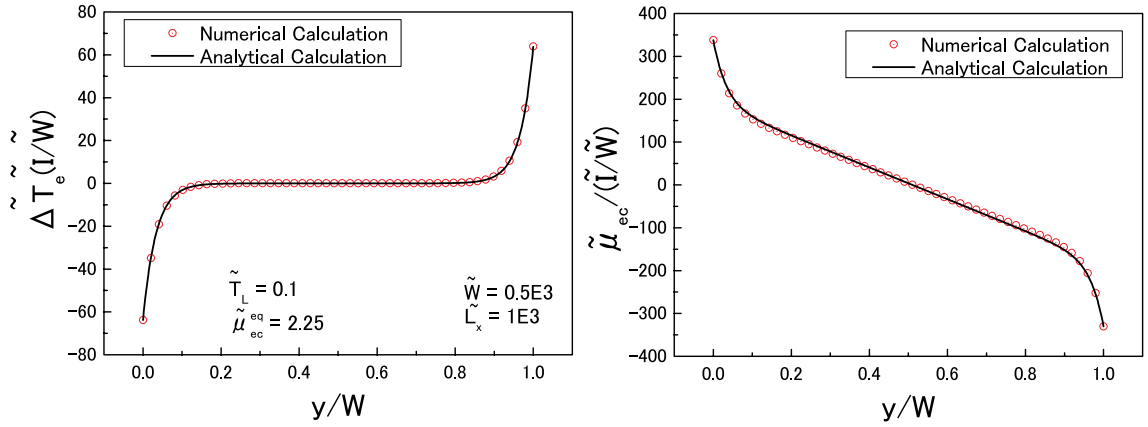

Figure 5.6: Spatial variations of the electron temperature and the electrochemical potential for $\tilde{L_x} = 1.0 \times 10^3$, $\tilde{W} = 0.5 \times 10^3$, $\tilde{T}_{\rm L} = 0.1$ and $\tilde{\mu}_{\rm ec}^{\rm eq} = 2.25$.

Chapter 6

Quantum Hall Systems with Potential Steps

6.1 Electrochemical Potential in the Isothermal Case

I consider the system, in which the potential in equilibrium has a dependence on x. It is difficult to solve eq.(4.5) and eq.(4.6) analytically in this system. Therefore first I simplify the system to calculate analytically. To simplify the system, I consider the system in the isothermal condition by putting $C_{\rm p} \to \infty$. This means that the electron temperature is equal to the lattice temperature because eq.(4.4) is written as

$$\frac{\boldsymbol{\nabla} \cdot \boldsymbol{j}_q^{\rm tr}}{C_{\rm p}} = T_{\rm e} - T_{\rm L}. \tag{6.1}$$

Therefore eq.(2.31) and eq.(2.32) can be written as

$$j_{nx}^{\rm tr}(\boldsymbol{r}, t) = -L_{xx}^{11}\nabla_x \mu_{\rm ec} + L_{yx}^{11}\nabla_y \mu_{\rm ec}, \tag{6.2}$$

$$j_{ny}^{\rm tr}(\boldsymbol{r}, t) = -L_{yx}^{11}\nabla_x \mu_{\rm ec} - L_{xx}^{11}\nabla_y \mu_{\rm ec}. \tag{6.3}$$

Using these equations, the equation about the conservation of the electron number is rewritten as

$$0 = -\frac{\partial L_{xx}^{11}}{\partial x}\nabla_x \mu_{\rm ec} + \frac{\partial L_{yx}^{11}}{\partial x}\nabla_y \mu_{\rm ec} - L_{xx}^{11}\nabla_x^2 \mu_{\rm ec} - L_{xx}^{11}\nabla_y^2 \mu_{\rm ec}. \tag{6.4}$$

Similarly, the boundary conditions can be rewritten to be

$$0 = -L_{yx}^{11}\nabla_x \mu_{\rm ec} - L_{xx}^{11}\nabla_y \mu_{\rm ec}. \tag{6.5}$$

6.1.1 Analytical Results in the Limit of the Slowly-Varying Potential

In this subsection, I consider the system in which the variation length scale λ is long so that

$$\nabla_x j_{nx}^{\rm tr} = 0, \nabla_x \nabla_y \mu_{\rm ec} = 0. \tag{6.6}$$

Using the equation of conservation and boundary conditions, I obtain

$$j_{ny}^{\rm tr} = 0. \ (-W/2 < y < W/2) \tag{6.7}$$

Then using eq.(6.2) and eq.(6.3), $\nabla_x \mu_{\rm ec}$ and $\nabla_y \mu_{\rm ec}$ are written as

$$\nabla_x \mu_{\rm ec} = -\frac{L_{yy}^{11}}{(L_{yy}^{11})^2 + (L_{yx}^{11})^2} j_{nx}^{\rm tr}, \tag{6.8}$$

$$\nabla_y \mu_{\rm ec} = \frac{L_{yx}^{11}}{(L_{yy}^{11})^2 + (L_{yx}^{11})^2} j_{nx}^{\rm tr}. \tag{6.9}$$

The gradient $\nabla_x \mu_{\rm ec}$ is independent of y since $\nabla_y \nabla_x \mu_{\rm ec} = \nabla_x \nabla_y \mu_{\rm ec} = 0$. Therefore $j^{\rm tr}_{nx}$ is also independent of y. Integrating $j^{\rm tr}_{nx}$, I obtain the equation :

$$\int_{-W/2}^{W/2} j^{\rm tr}_{nx} dy = j^{\rm tr}_{nx} W = I. \tag{6.10}$$

I obtain $\nabla_x \mu_{\rm ec}$ and $\nabla_y \mu_{\rm ec}$ to be

$$\nabla_x \mu_{\rm ec} = -\frac{(I/W) L^{11}_{yy}}{(L^{11}_{yy})^2 + (L^{11}_{yx})^2}, \tag{6.11}$$

$$\nabla_y \mu_{\rm ec} = \frac{(I/W) L^{11}_{yx}}{(L^{11}_{yy})^2 + (L^{11}_{yx})^2}. \tag{6.12}$$

6.1.2 Analytical Results in the Limit of the Narrow Width

In this subsection, I consider the system which is so narrow that only terms in the lowest order of W should be retained.

Using the Taylar expantion, $j^{\rm tr}_{ny}$ is written in this approximation as

$$j^{\rm tr}_{ny} \sim j^{\rm tr}_{ny}|_{y=W/2}, \tag{6.13}$$

and $j^{\rm tr}_{ny}$ is independent of y. Using boundary conditions, $j^{\rm tr}_{ny}$ is written as

$$j^{\rm tr}_{ny} = 0. \ (-W/2 \ \leq \ y \ \leq \ W/2) \tag{6.14}$$

Therefore using the discussion of the section (6.1.1), I can derive $\nabla_x \mu_{\rm ec}$ and $\nabla_y \mu_{\rm ec}$:

$$\nabla_x \mu_{\rm ec} = -\frac{(I/W) L^{11}_{yy}}{(L^{11}_{yy})^2 + (L^{11}_{yx})^2}, \tag{6.15}$$

$$\nabla_y \mu_{\rm ec} = \frac{(I/W) L^{11}_{yx}}{(L^{11}_{yy})^2 + (L^{11}_{yx})^2}. \tag{6.16}$$

The electrochemical potential in the limit of $W \to 0$ is equal to the electrochemical potential in the Limit of $\lambda \to \infty$.

6.1.3 Numerical Results in the Narrow Width Case

I calculate the variations of $\tilde{\mu}_{\rm ec}$. The chemical potential in the region A $\tilde{\mu}^{\rm eq}_A = \tilde{\mu}^{\rm eq}_{\rm ec} = 2.25$, the potential difference $\Delta \tilde{V} = 0.5$, the chemical potential in the region B $\tilde{\mu}^{\rm eq}_B = \tilde{\mu}^{\rm eq}_{\rm ec} - \Delta \tilde{V} = 1.75$, $\tilde{T}_{\rm L} = 0.1$,$W = 0.01 \times 10^4$, $\tilde{\lambda} = 0.25 \times 10^4$ and $\tilde{L}_x = 1 \times 10^4$ are used. The result is shown in Fig.6.1. This result is consistent with the result of the one-dimensional calculation as shown in Fig.6.2 and Fig.6.3.

6.1.4 Numerical Results : W Dependence

The one-dimensional variation of $\mu_{\rm ec}$ can be derived analytically. I can't however derive W dependence of the variation of $\mu_{\rm ec}$ analytically. Therefore I derive it numerically. The variation of $\mu_{\rm ec}$ has negligible dependence on the number of the sites as shown in Fig.6.4. Fig.6.5 suggests that the variation of $\mu_{\rm ec}$ peculiar to a two-dimensional system exists.

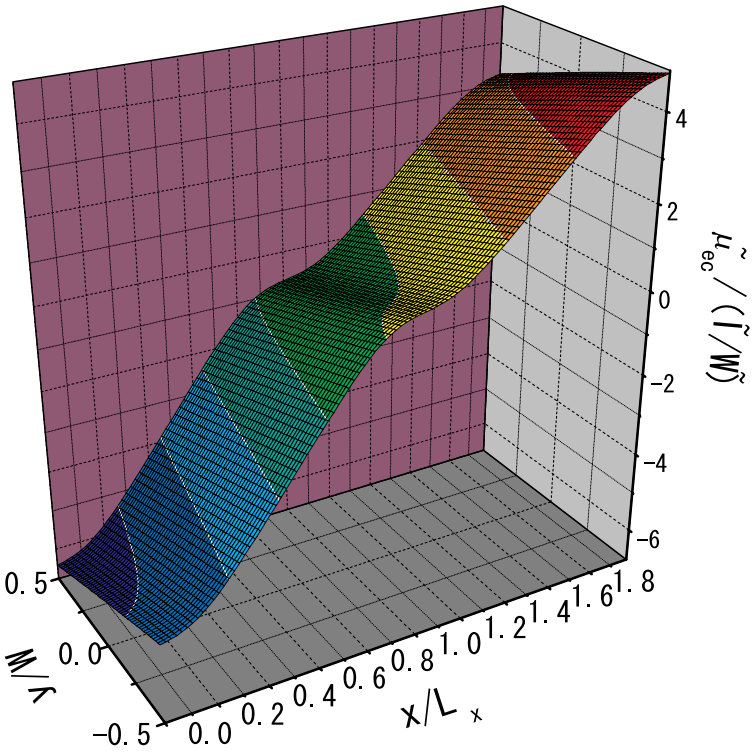

Figure 6.1: Spatial variations of $\tilde{\mu}_{\rm ec}$.

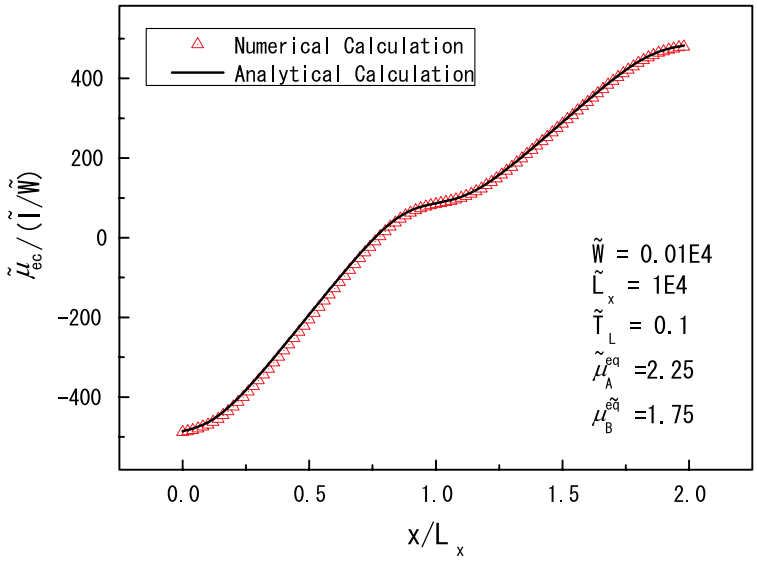

Figure 6.2: Variations of $\tilde{\mu}_{\rm ec}$ at $\tilde{y} = 0$ (center). The result of the analytical calculation in the limit of $\tilde{W} \to 0$ is consistent with that of the numerical calculation.

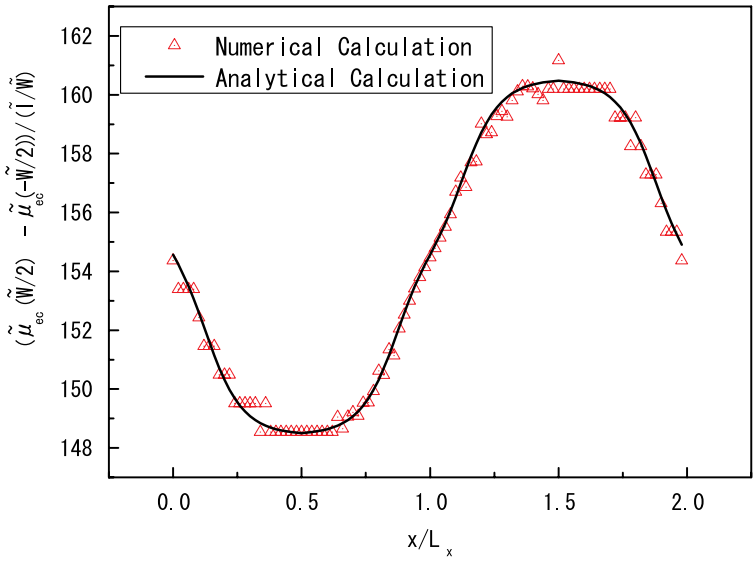

Figure 6.3: Spatial variations of $(\tilde{\mu}_{\rm ec}(\tilde{W}/2) - \tilde{\mu}_{\rm ec}(-\tilde{W}/2))/(\tilde{I}/\tilde{W})$. The result of the analytical calculation in the limit of $\tilde{W} \to 0$ is consistent with that of the numerical calculation.

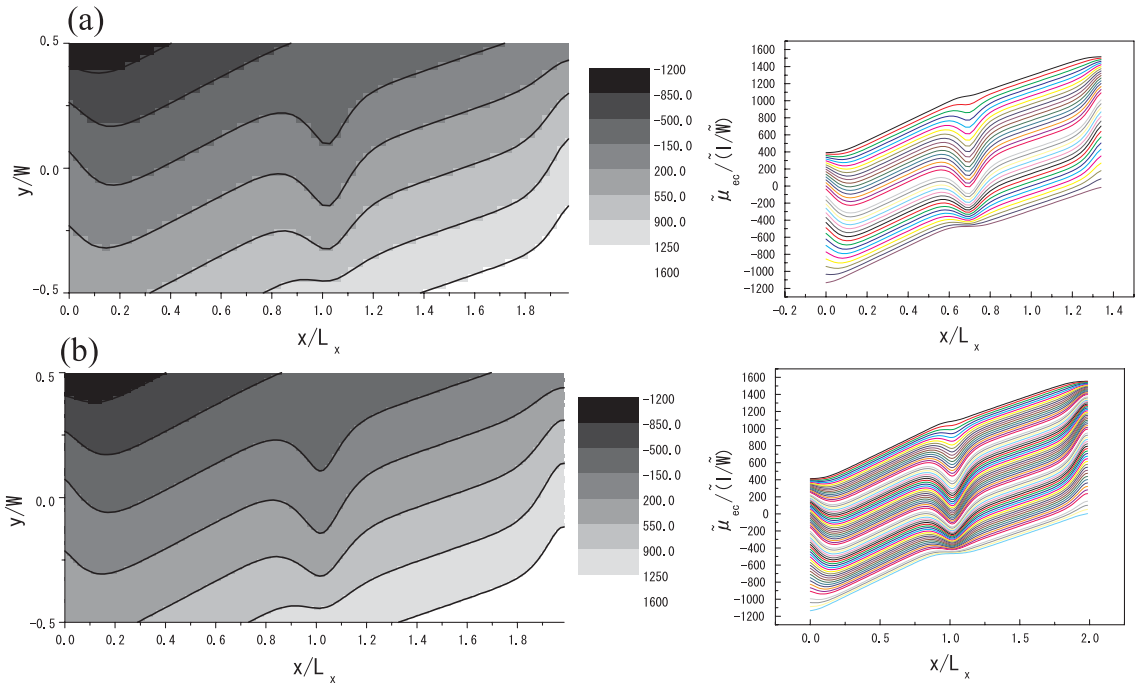

Figure 6.4: N dependence of the electrochemical potential. The spatial variations for $\tilde{W} = 0.1 \times 10^4$, $\tilde{T}_{\rm L} = 0.1$, $\tilde{\lambda} = 0.15 \times 10^4$, $\tilde{\mu}_{\rm A} = 2.25$, $\tilde{\mu}_{\rm B} = 1.75$, and $\tilde{L_x} = 1.0 \times 10^4$. The lattice constant Δx is (a)$\Delta\tilde{x} = \tilde{L_x}/N = 0.03 \times 10^4$ and (b)$\Delta\tilde{x} = \tilde{L_x}/N = 0.015 \times 10^4$. In the left side is an equipotential line of $\tilde{\mu}_{\rm ec}$. In the right side is the variation at each y in the x direction.

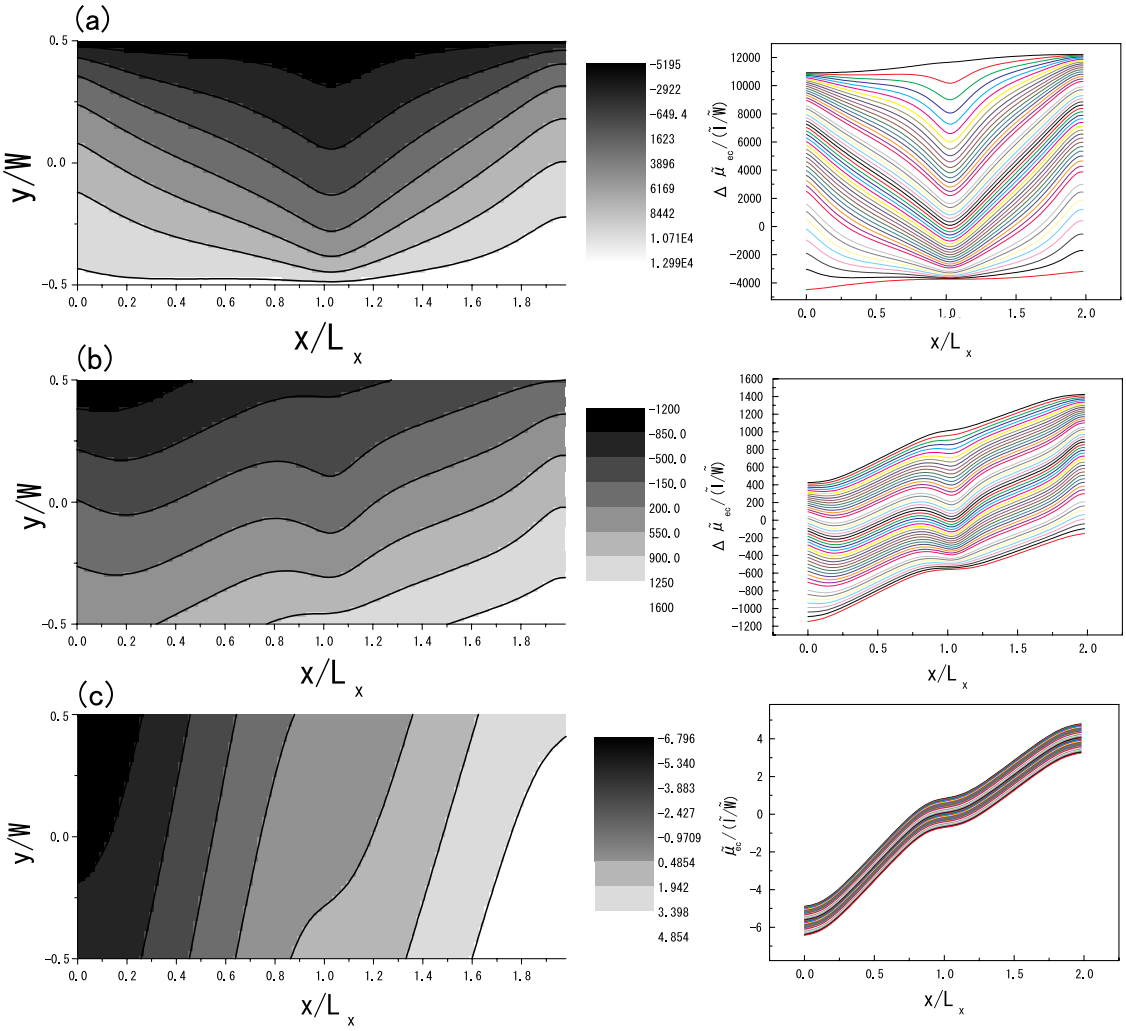

Figure 6.5: W dependence of the electrochemical potential : the spatial variations for $\tilde{L_x} = 1.0 \times 10^4$, $\tilde{\lambda} = 0.25 \times 10^4$, $\tilde{T_{\rm L}} = 0.1$, $\tilde{\mu}_{\rm A} = 2.25$, and $\tilde{\mu}_{\rm B} = 1.75$. (a):$\tilde{W} = 1.0 \times 10^4$,(b):$\tilde{W} = 0.1 \times 10^4$,(c):$\tilde{W} = 0.01 \times 10^4$.

6.1.5 Numerical Results : Dependences on Other Parameters

There are results from Fig.6.5 to Fig.6.8. One parameter is changed in each result. There are the results in the standard parameters for $\tilde{L_x} = 1.0 \times 10^4$, $\tilde{\lambda} = 0.15 \times 10^4$, $\tilde{T_{\rm L}} = 0.1$, $\tilde{\mu}_{\rm A} = 2.25$, $\tilde{\mu}_{\rm B} = 1.75$, and $\tilde{W} = 0.1 \times 10^4$ in the center of the each figure. As shown in results, the variation of $\mu_{\rm ec}$ peculiar to a two-dimensional system occurs near the boundaries ($x = 0.L_x$).

Increasing $\tilde{D_0}$ or $\tilde{T_{\rm L}}$, the variation of $\mu_{\rm ec}$ peculiar to a two-dimensional system becomes small as shown in Fig.6.6. Increasing $\Delta\tilde{V}$ or decreasing $\tilde{\lambda}$, the electric field concentrates more at the hot spot as shown in Fig.6.7. Fig.6.8 shows that the concentration of the electric field is only near the boundary($x = 0, L_x$).

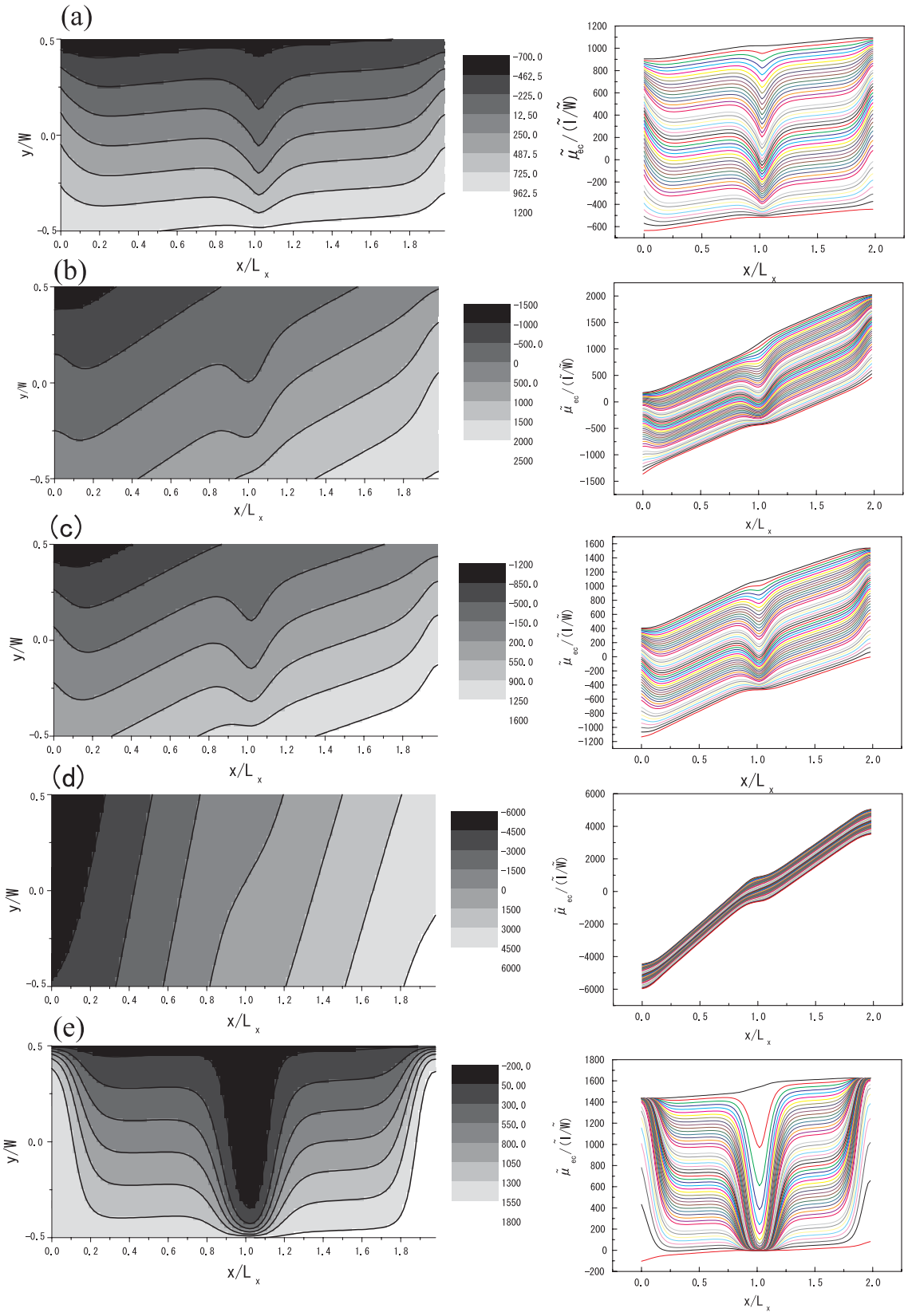

Figure 6.6: $T_{\rm L}$ dependence is in the upper side and the D_0 dependence is in the lower side. The spatial variations of $\tilde{\mu}_{\rm ec}$ for $\tilde{L_x} = 1.0 \times 10^4$, $\tilde{W} = 0.1 \times 10^4$, $\tilde{\lambda} = 0.15 \times 10^4$, $\tilde{\mu}_{\rm A} = 2.25$, and $\tilde{\mu}_{\rm B} = 1.75$. The lattice temperature is $\tilde{T_{\rm L}} = 0.05$ in (a), $\tilde{T_{\rm L}} = 0.2$ in (b), and $\tilde{T_{\rm L}} = 0.1$ in (c), (d) and (e). The transition rate is $\tilde{D_0} = 0.005$ in (a), (b) and (c), $\tilde{D_0} = 0.05$ in (d), and $\tilde{D_0} = 0.0005$ in (e).

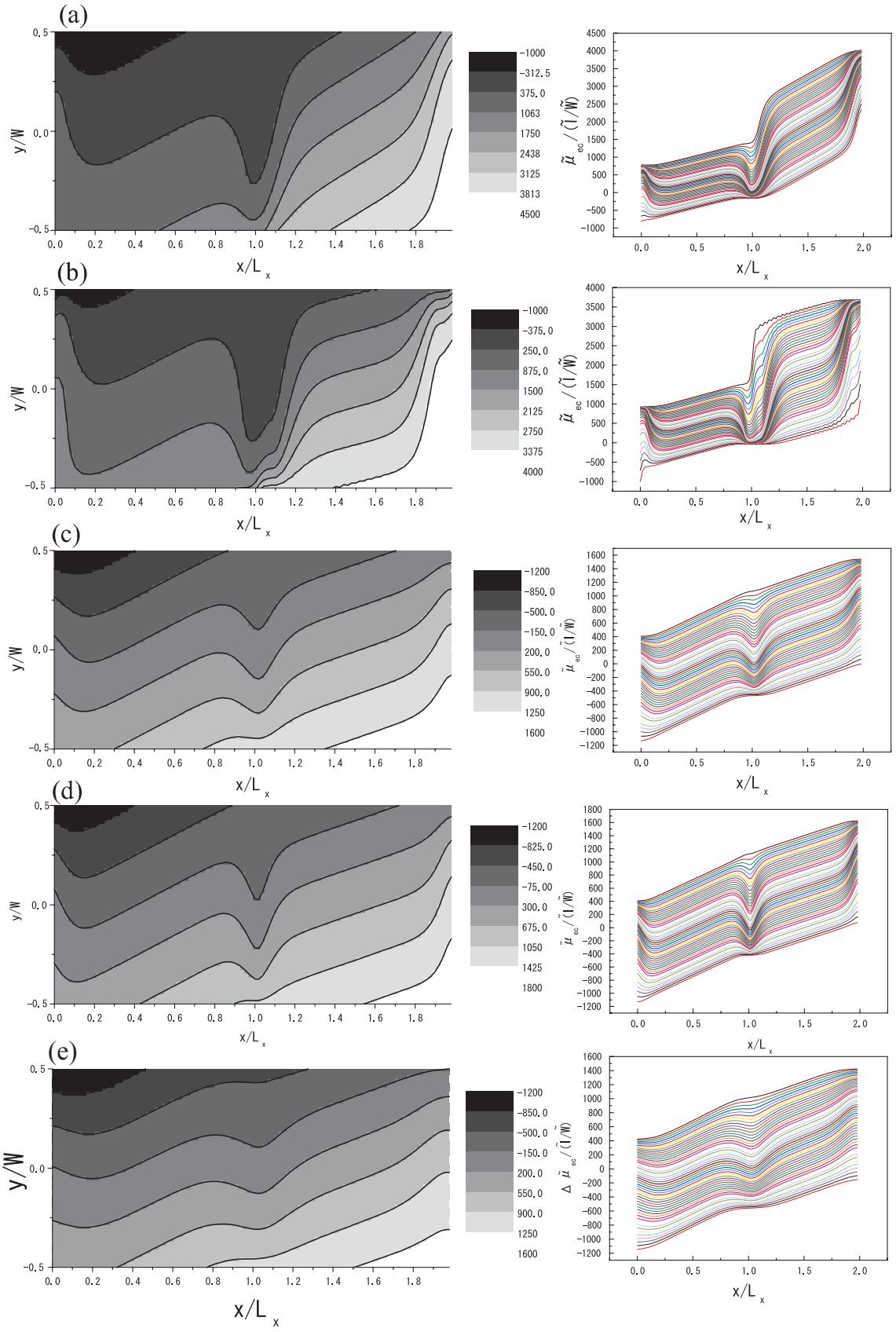

Figure 6.7: ΔV dependence is in the upper side and the λ dependence is in the lower side. The spatial variations of $\tilde{\mu}_{\rm ec}$ for $\tilde{L}_x = 1.0 \times 10^4$, $\tilde{W} = 0.1 \times 10^4$, $\tilde{T}_{\rm L} = 0.1$, and $\tilde{\mu}_{\rm A} = 2.25$. The chemical potential is $\tilde{\mu}_{\rm B} = 1.25$ in (a), $\tilde{\mu}_{\rm B} = 0.75$ in (b), and $\tilde{\mu}_{\rm B} = 1.75$ in (c), (d) and(e). The potential variation length is $\tilde{\lambda} = 0.15 \times 10^4$ in (a), (b) and (c), $\tilde{\lambda} = 0.10 \times 10^4$ in (d), and $\tilde{\lambda} = 0.25 \times 10^4$ in (e).

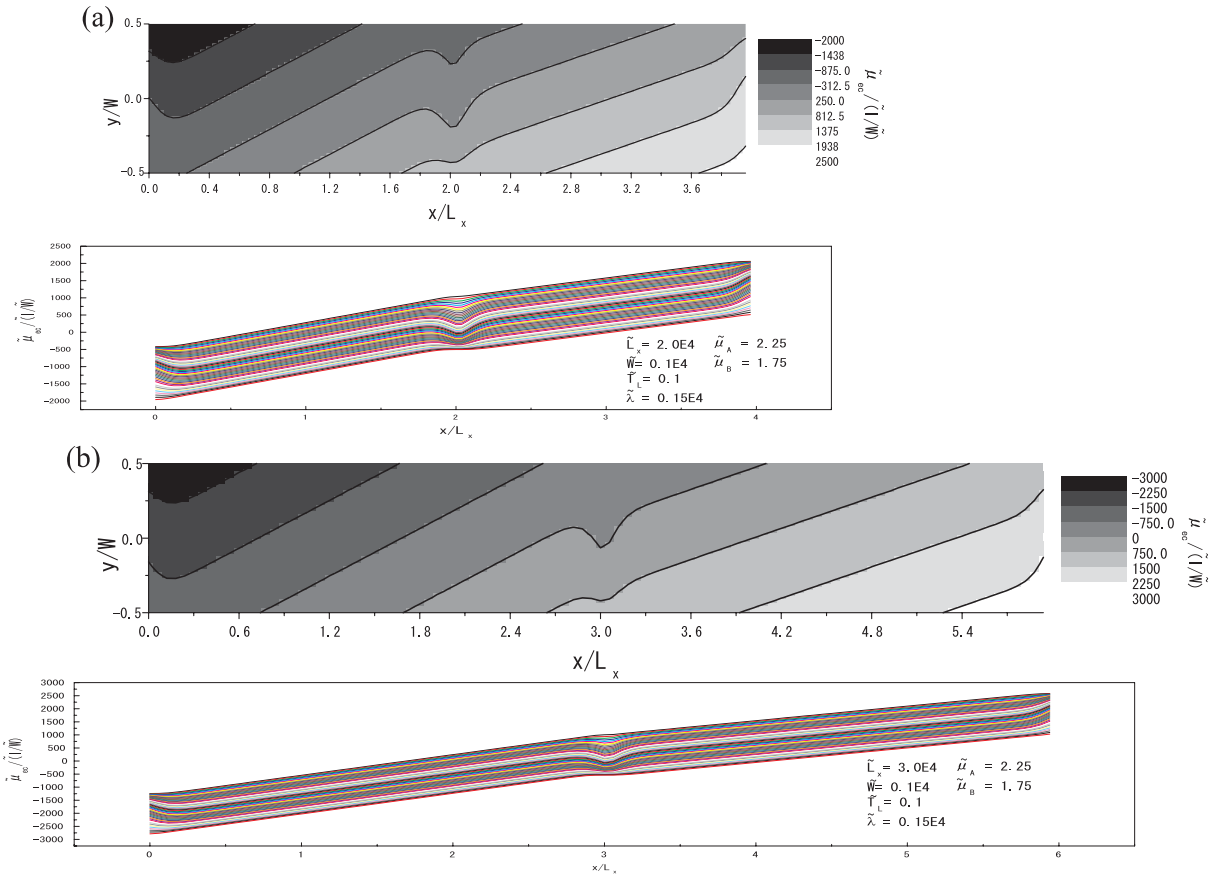

Figure 6.8: L_x dependence of the electrochemical potential. The spatial variations for $\tilde{W} = 0.1 \times 10^4$, $\tilde{T_{\rm L}} = 0.1$, $\tilde{\lambda} = 0.15 \times 10^4$, $\tilde{\mu}_{\rm A} = 2.25$, $\tilde{\mu}_{\rm B} = 1.75$, and $\tilde{L_x} = 1.0 \times 10^4$. The length of the sample is (a)$\tilde{L_x} = 2.0 \times 10^4$ and (b)$\tilde{L_x} = 3.0 \times 10^4$.

6.2 Electron Temperature and the Electrochemical Potential:Numerical Calculation

6.2.1 Comparison with Analytical Result in the Limit of $W \ll \lambda_T$

In the limit of $W \ll \lambda_T$, I expect that the result of the two-dimensional numerical calculation is in agreement with that of the one-dimensional analytical calculation shown in Appendix. Fig.6.9-(a) shows that the variation of $\Delta T_{\rm e}$ of the numerical calculation in the case of small λ is in good agreement with that of $\Delta T_{\rm e}$ of the analytical calculation with discontinuous potential steps(see Appendix). Similarly, Fig.6.9-(b) shows that the variation of $\mu_{\rm ec}$ in the two-dimensional calculation is in agreement with that of $\mu_{\rm ec}$ in the one-dimensional calculation.

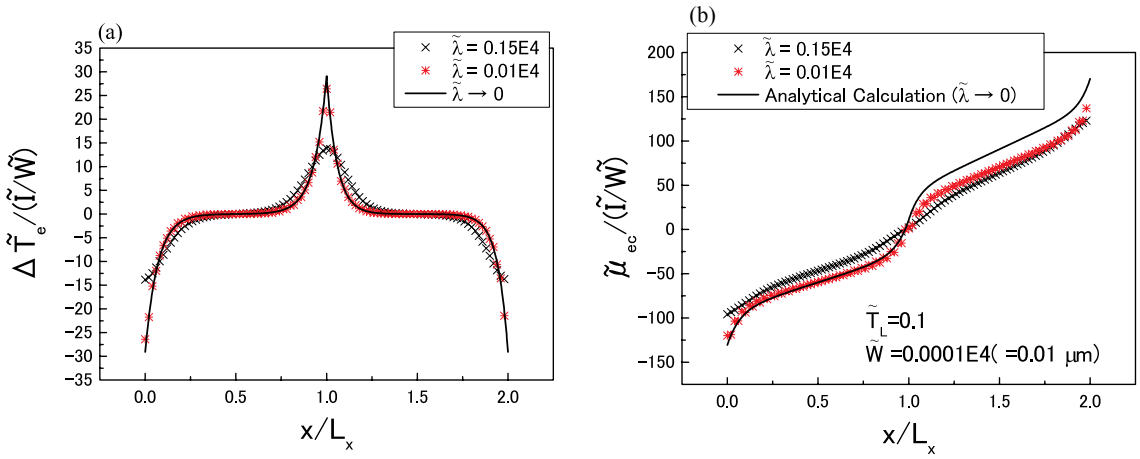

Figure 6.9: Spatial variation of (a) the electron temperature and (b) the electrochemical potential for $\tilde{L_x} = 1.0 \times 10^4$, $\tilde{W} = 0.0001 \times 10^4$, $\tilde{T_{\rm L}} = 0.1$, $\tilde{\mu}_{\rm A} = 2.25$, $\tilde{\mu}_{\rm B} = 1.75$ and $\tilde{\lambda}_T \sim 0.002 \times 10^4$.

6.2.2 Results

Fig.6.10 shows Ettingshausen Effect. The carriers are different in each region since the chemical potential in the region A is $\tilde{\mu} = 2.25$ and one in the region B is $\tilde{\mu} = 1.75$. Therefore the gradient of the electron temperature is reversed each region as shown in Fig.6.10 since the direction of the thermal current is different in each region. The maximum of $\Delta T_{\rm e}$ is estimated to be about $5K$ in the following parameters : $I/W = 0.1A/m$ and $B = 5T$.

I calculated the distribution of the electron temperature and the electrochemical potential in the following parameters : $\tilde{\mu}_{\rm ec}^{\rm eq} = 3.00$, $\Delta\tilde{V} = 1.0$, $\tilde{L_x} = 1.0 \times 10^4$, $\tilde{W} = 0.1 \times 10^4$, $\tilde{\lambda} = 0.1 \times 10^4$ and $\tilde{T_{\rm L}} = 0.1$. The filling factor is 6 in A and 4 in B, in agreement with the experiment by U. Klass et al.[14]. The result is shown in Fig.6.11. The electron temperature rises near the hot spot. The electric field concentrates near the hot spot. The maximum of $\Delta T_{\rm e}$ is estimated to be about $5K$ in the following parameters : $I/W = 0.1A/m$ and $B = 5T$.

There are results from Fig.6.14 to Fig.6.19. One parameter is changed in each result. As shown in results, the variation of $\mu_{\rm ec}$ peculiar to a two-dimensional system occurs near the boundaries ($x = 0.L_x$). The variations of $\mu_{\rm ec}$ and $T_{\rm e}$ have negligible dependence on the number of the sites as shown in Fig.6.12.

Increasing the width of the sample, we can recognize the two-dimensional behavior of the system. $j_{ny}^{\rm tr}$ can be neglected in the one-dimensional system but it can not be neglected in the two-dimensional system as shown in Fig.6.20. The current in the y direction causes the variation of $\mu_{\rm ec}$ from eq.(2.32).

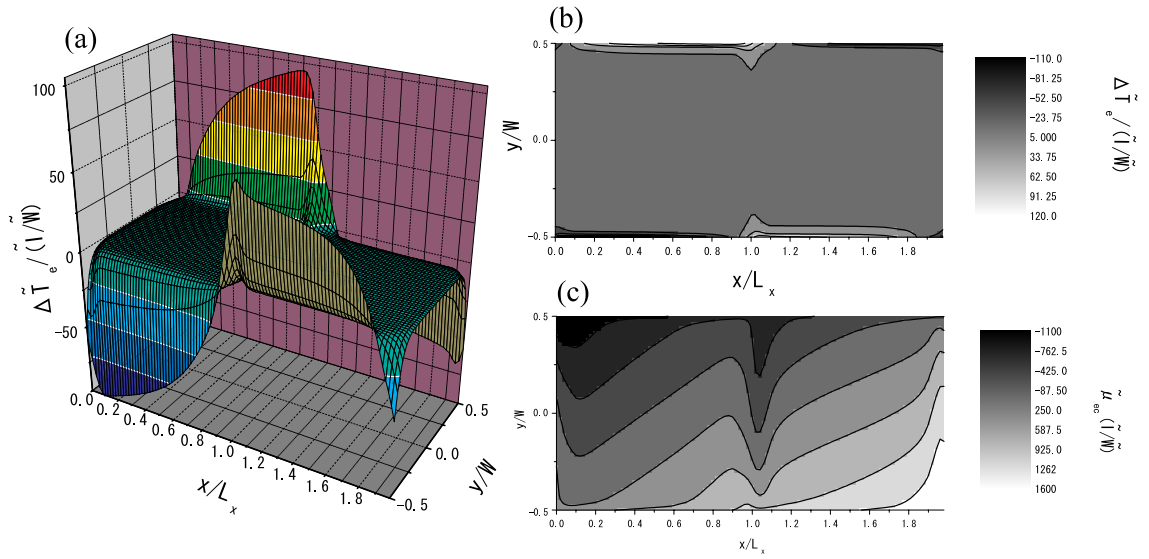

Figure 6.10: Spatial variations of $\tilde{T}_{\rm e}$ and $\tilde{\mu}_{\rm ec}$ in the following parameters : $\tilde{L_x} = 1.0{\times}10^4$, $\tilde{W} = 0.1{\times}10^4$, $\tilde{\lambda} = 0.1 \times 10^4$, $\tilde{T_{\rm L}} = 0.1$, $\tilde{\mu}_A^{\rm eq} = 2.25$, $\tilde{\mu}_B^{\rm eq} = 1.75$ and $N = 50$.The lattice constant in the numerical calculation is $\tilde{d} = \tilde{L_x}/N = 0.02 \times 10^4$. (a) and (b) are the spatial variations of $\tilde{T}_{\rm e}$. (c) is the spatial variation of $\tilde{\mu}_{\rm ec}$.

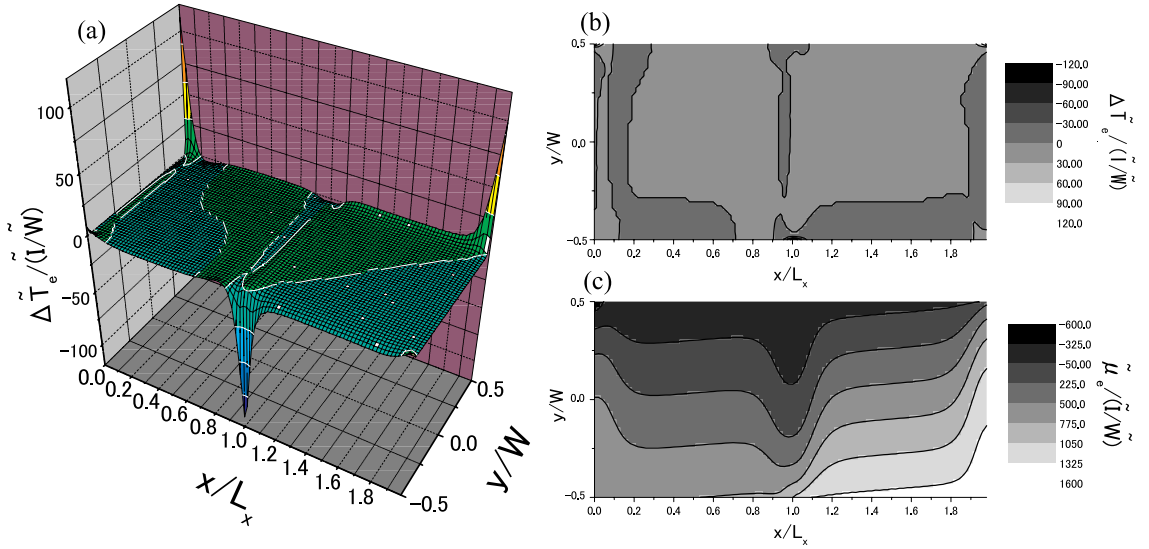

Figure 6.11: Spatial variations of $\tilde{T}_{\rm e}$ and $\tilde{\mu}_{\rm ec}$ in the following parameters : $\tilde{L_x} = 1.0{\times}10^4$, $\tilde{W} = 0.1{\times}10^4$, $\tilde{\lambda} = 0.15 \times 10^4$, $\tilde{T_{\rm L}} = 0.1$, $\tilde{\mu}_A^{\rm eq} = 3.00$, $\tilde{\mu}_B^{\rm eq} = 2.00$ and $N = 50$.The lattice constant in the numerical calculation is $\tilde{d} = \tilde{L_x}/N = 0.02 \times 10^4$. (a) and (b) are the spatial variations of $\tilde{T}_{\rm e}$. (c) is the spatial variation of $\tilde{\mu}_{\rm ec}$.

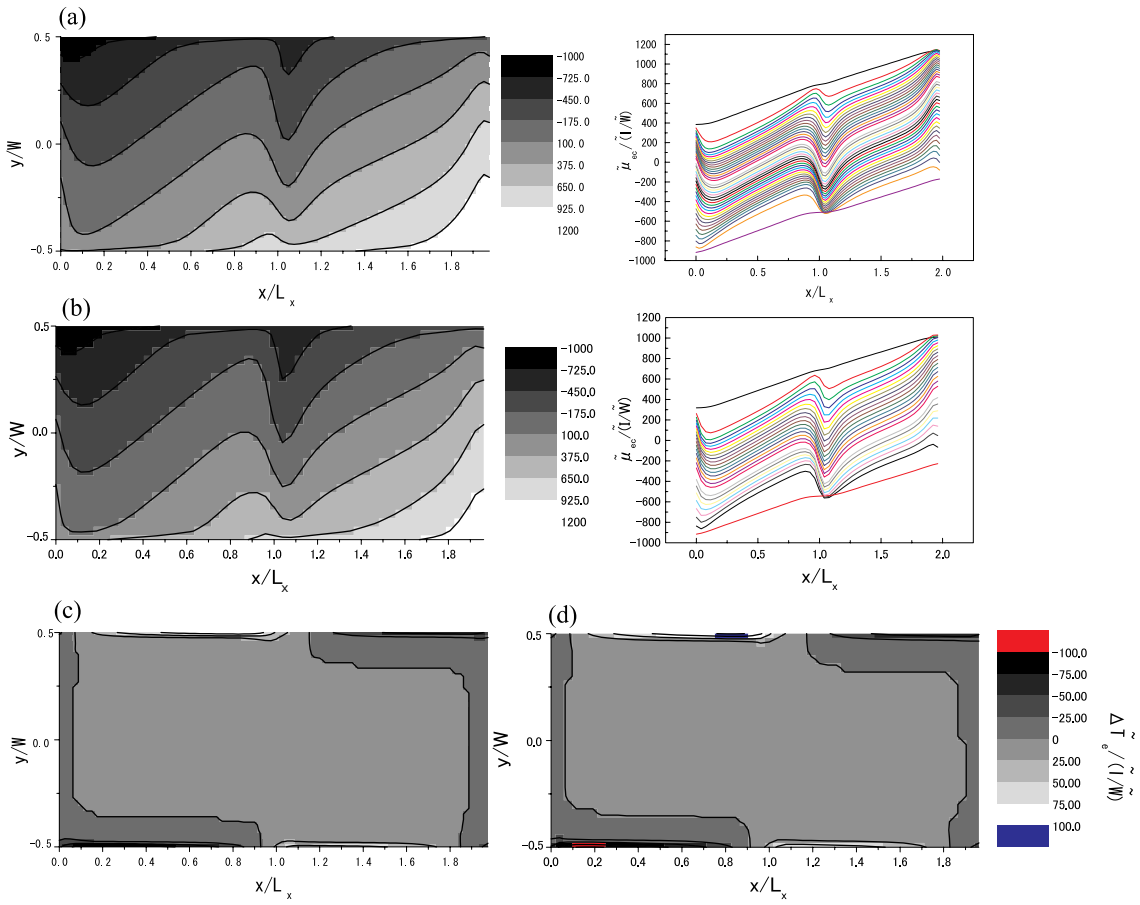

Figure 6.12: N dependence of the electrochemical potential and the electron temperature. The spatial variations for $\tilde{L_x} = 1.0 \times 10^4$, $\tilde{W} = 0.1 \times 10^4$, $\tilde{\lambda} = 0.15 \times 10^4$, $\tilde{T_{\rm L}} = 0.1$, $\tilde{\mu}_{\rm A} = 2.25$ and $\tilde{\mu}_{\rm B} = 1.75$. The lattice constant $\Delta\tilde{x}$ is (a)(c)$\Delta x = \tilde{L_x}/N = 0.040 \times 10^4$ and (b)(d)$\Delta\tilde{x} = \tilde{L_x}/N = 0.020 \times 10^4$. In the left side is an equipotential line of $\tilde{\mu}_{\rm ec}$. In the right side is the variation at each y in the x direction.

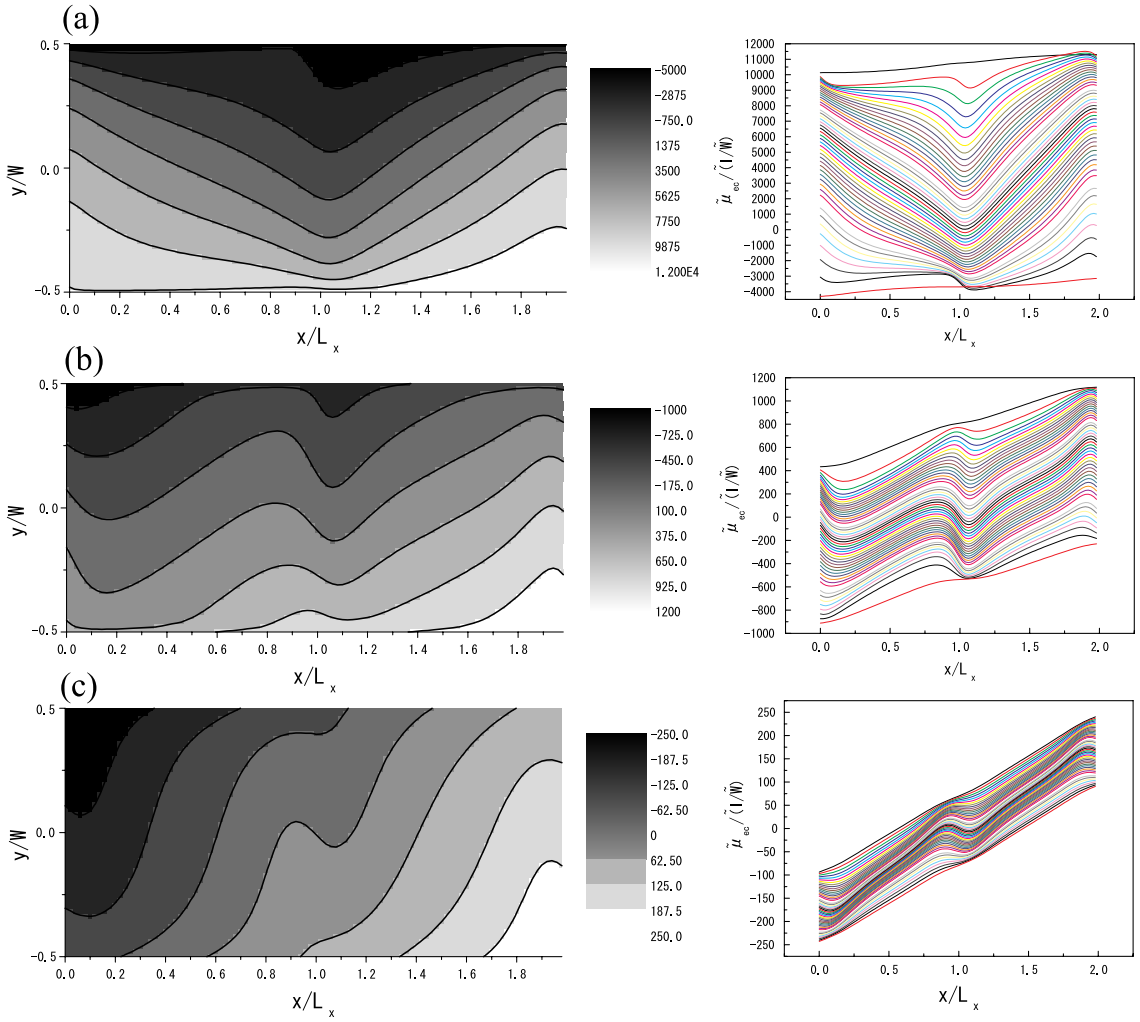

Figure 6.13: W dependence of the electrochemical potential : the spatial variations for $\tilde{L_x} = 1.0 \times 10^4$, $\tilde{\lambda} = 0.25 \times 10^4$, $\tilde{T_{\rm L}} = 0.1$, $\tilde{\mu}_{\rm A} = 2.25$, and $\tilde{\mu}_{\rm B} = 1.75$. (a):$\tilde{W} = 1.0 \times 10^4$,(b):$\tilde{W} = 0.1 \times 10^4$,(c):$\tilde{W} = 0.01 \times 10^4$. In the left side is an equipotential line of $\tilde{\mu}_{\rm ec}$. In the right side is the variation at each y in the x direction.

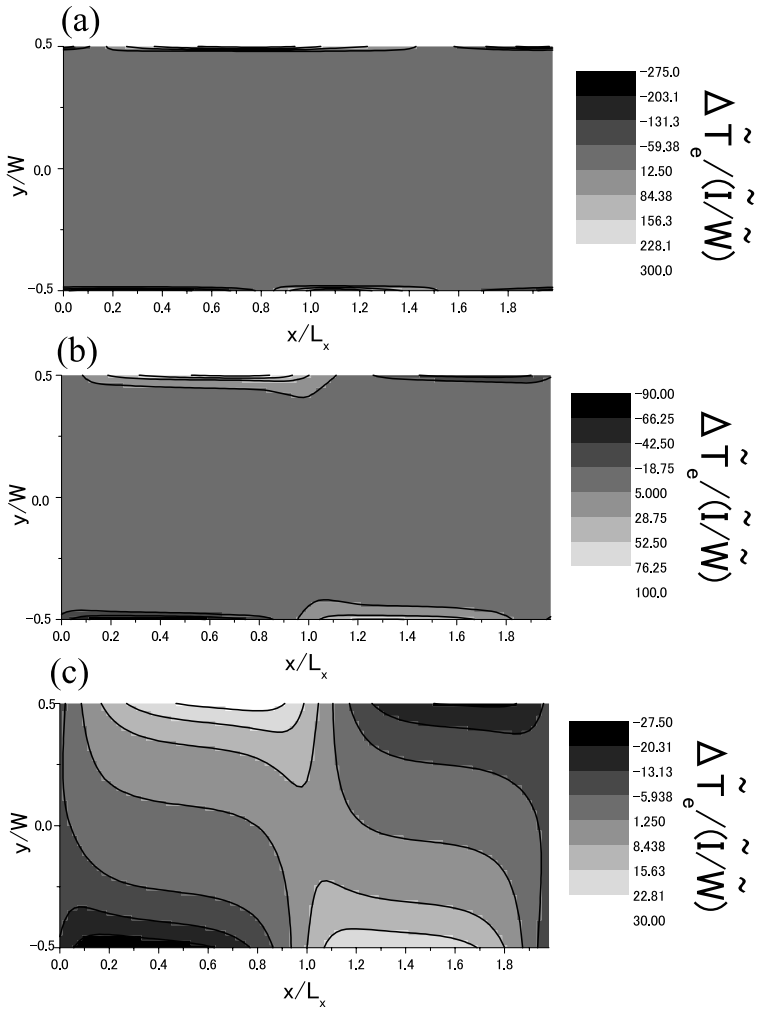

Figure 6.14: W dependence of the electron temperature : the spatial variations for $\tilde{L_x} = 1.0 \times 10^4$, $\tilde{\lambda} = 0.25 \times 10^4$, $\tilde{T_{\rm L}} = 0.1$, $\tilde{\mu}_{\rm A} = 2.25$, and $\tilde{\mu}_{\rm B} = 1.75$. (a):$\tilde{W} = 1.0 \times 10^4$,(b):$\tilde{W} = 0.1 \times 10^4$,(c):$\tilde{W} = 0.01 \times 10^4$.

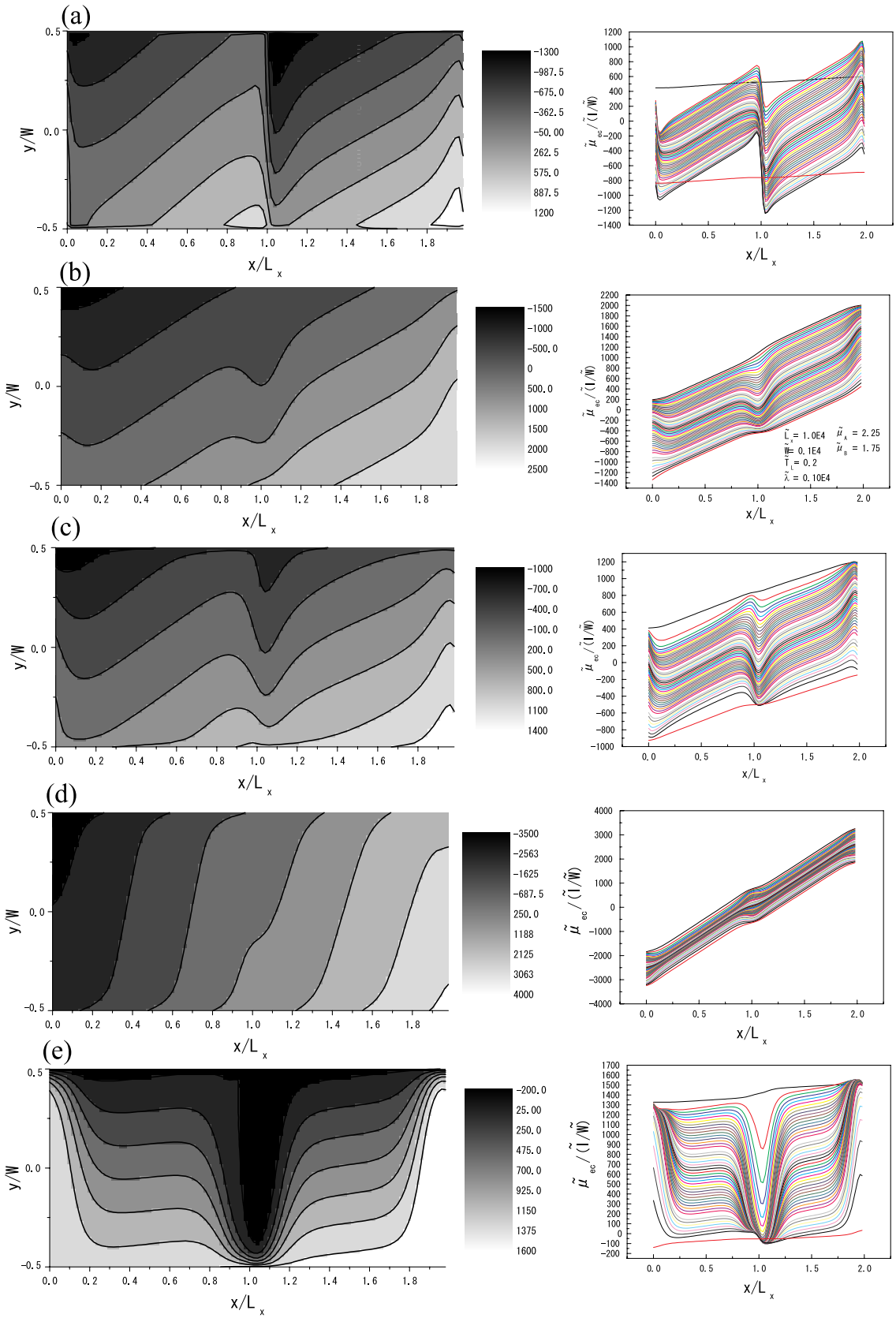

Figure 6.15: $T_{\rm L}$ dependence is in the upper side and the D_0 dependence is in the lower side. The spatial variations of $\tilde{\mu}_{\rm ec}$ for $\tilde{L_x} = 1.0 \times 10^4$, $\tilde{W} = 0.1 \times 10^4$, $\tilde{\lambda} = 0.15 \times 10^4$, $\tilde{\mu}_{\rm A} = 2.25$, and $\tilde{\mu}_{\rm B} = 1.75$. The electron temperature is $\tilde{T_{\rm L}} = 0.05$ in (a), $\tilde{T_{\rm L}} = 0.2$ in (b), and $\tilde{T_{\rm L}} = 0.1$ in (c), (d) and(e). The transition rate is $\tilde{D_0} = 0.005$ in (a), (b) and (c), $\tilde{D_0} = 0.05$ in (d), and $\tilde{D_0} = 0.0005$ in (e).

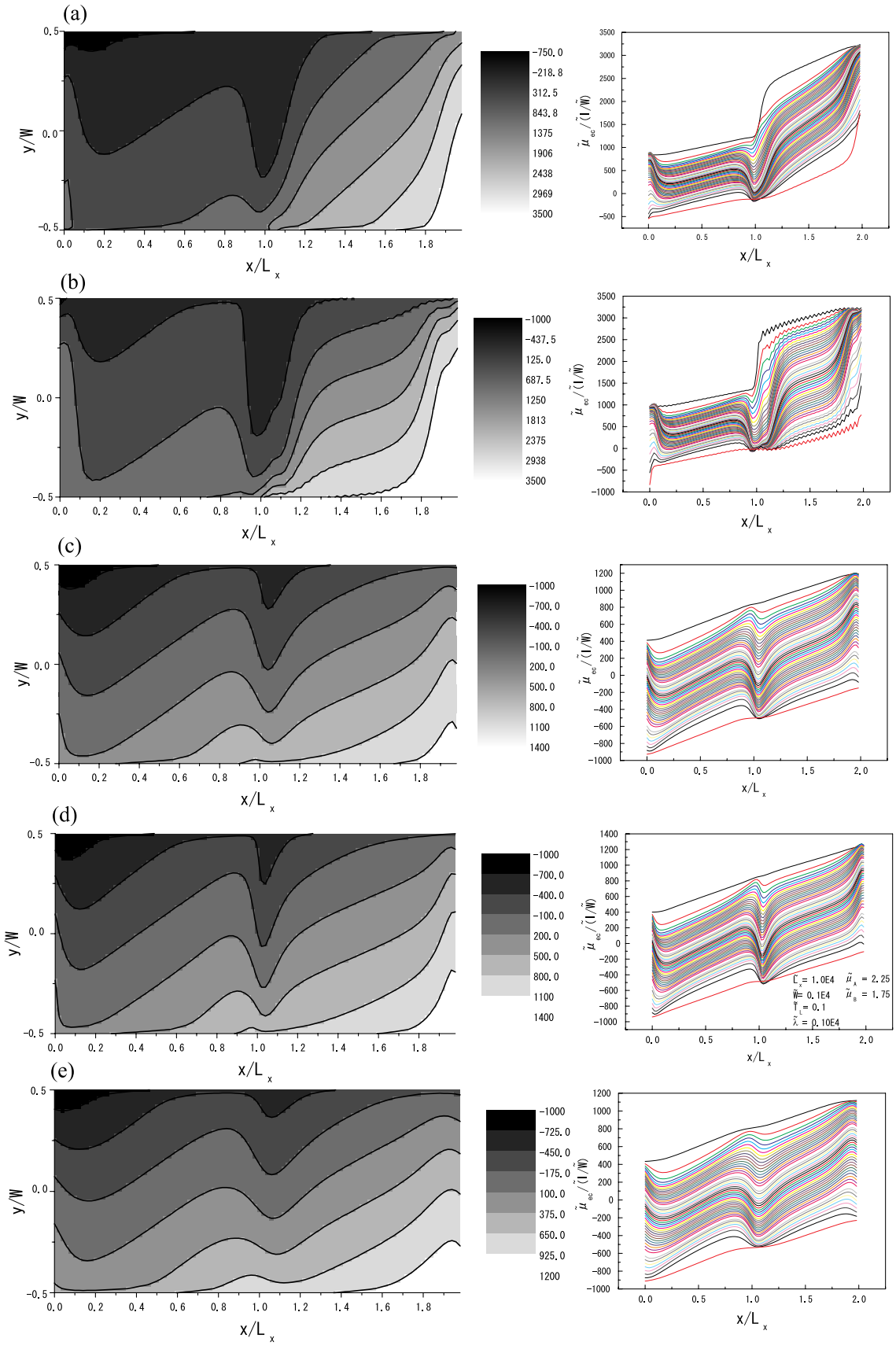

Figure 6.16: ΔV dependence is in the upper side and the λ dependence is in the lower side. The spatial variations of $\tilde{\mu}_{\rm ec}$ for $\tilde{L_x} = 1.0 \times 10^4$, $\tilde{W} = 0.1 \times 10^4$, $\tilde{T_{\rm L}} = 0.1$ and $\tilde{\mu}_{\rm A} = 2.25$. The chemical potential is $\tilde{\mu}_{\rm B} = 1.25$ in (a), $\tilde{\mu}_{\rm B} = 0.75$ in (b), and $\tilde{\mu}_{\rm B} = 1.75$ in (c), (d) and (e). The potential variation length is $\tilde{\lambda} = 0.15$ in (a), (b) and (c), $\tilde{\lambda} = 0.10$ in (d), and $\tilde{\lambda} = 0.25$ in (e).

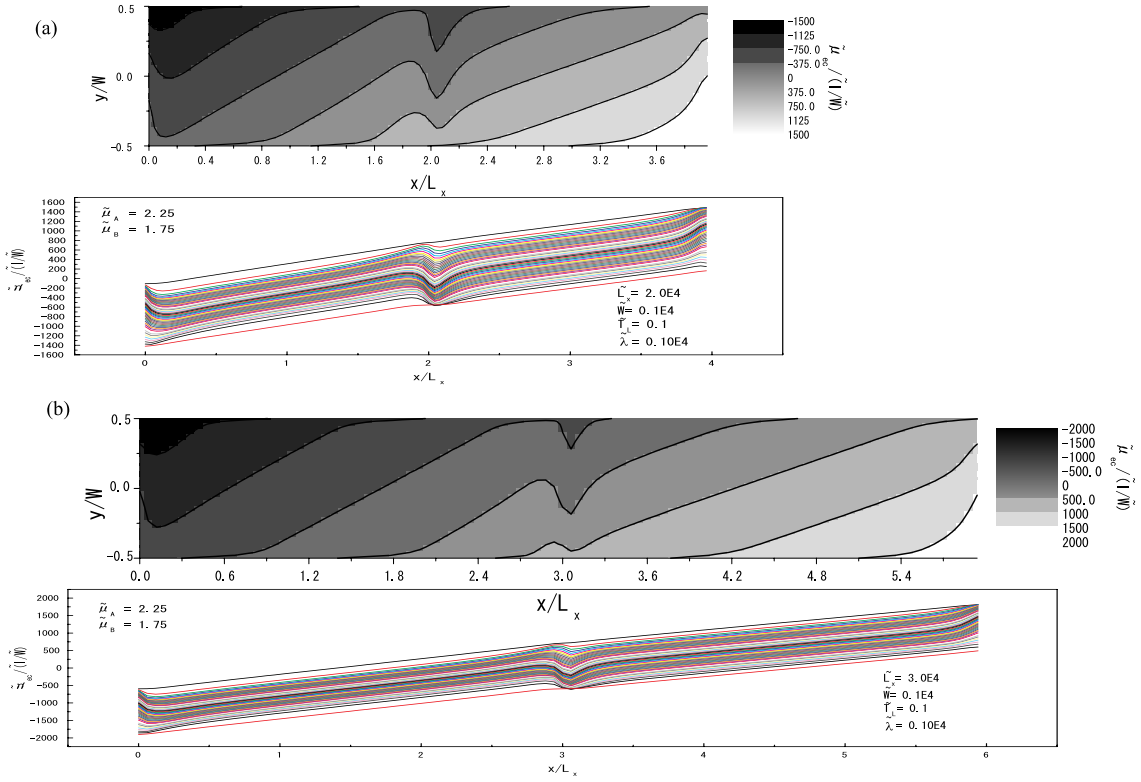

Figure 6.17: L_x dependence of the electrochemical potential. The spatial variations for $\tilde{W} = 0.1 \times 10^4$, $\tilde{T_{\rm L}} = 0.1$, $\tilde{\lambda} = 0.15 \times 10^4$, $\tilde{\mu}_{\rm A} = 2.25$, $\tilde{\mu}_{\rm B} = 1.75$, and $\tilde{L_x} = 1.0 \times 10^4$. The length of the sample is (a)$\tilde{L_x} = 2.0 \times 10^4$ and (b)$\tilde{L_x} = 3.0 \times 10^4$.

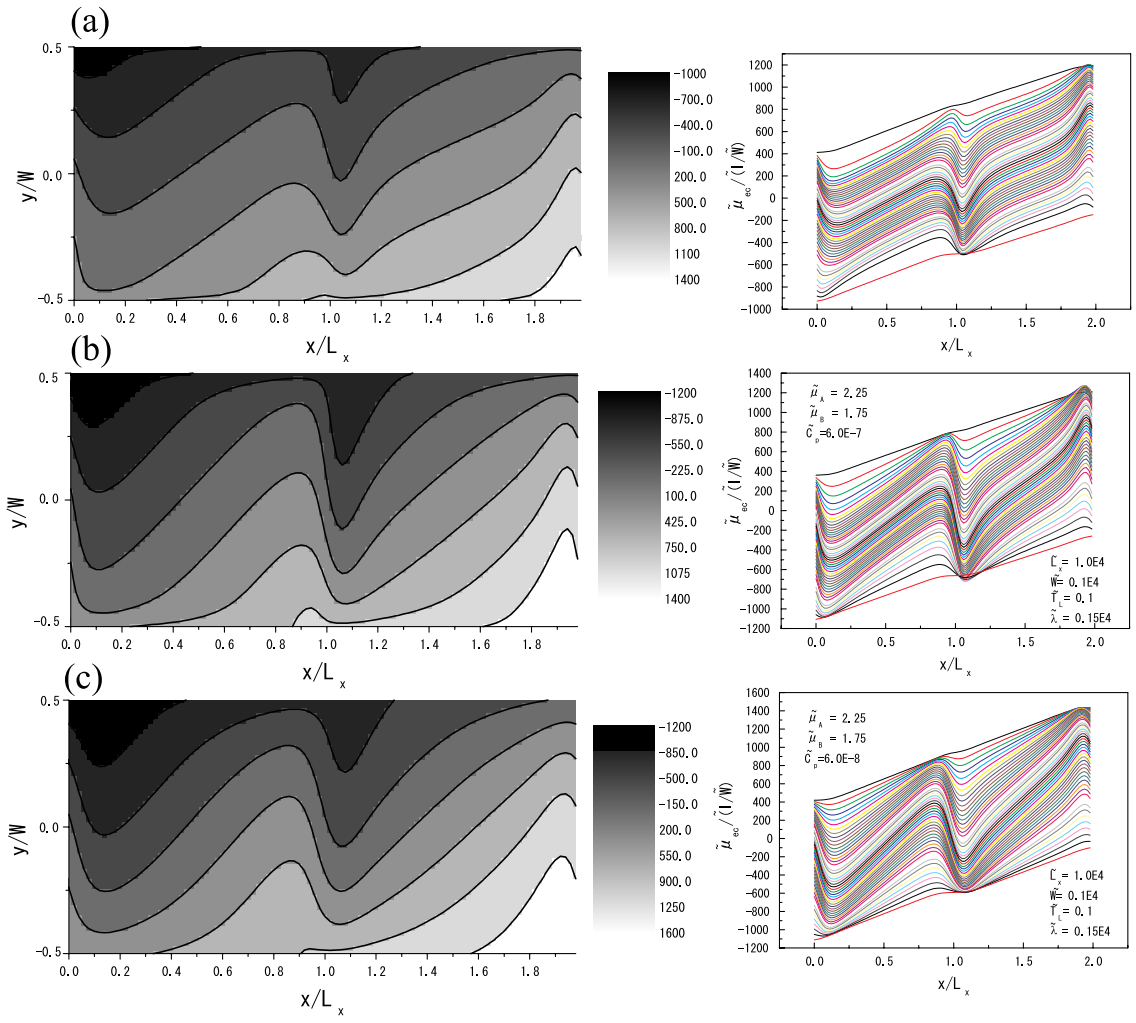

Figure 6.18: $C_{\rm p}$ dependence of the electrochemical potential. The spatial variations for $\tilde{L_x} = 1.0 \times 10^4$, $\tilde{W} = 0.1 \times 10^4$, $\tilde{T_{\rm L}} = 0.1$, $\tilde{\lambda} = 0.15 \times 10^4$, $\tilde{\mu}_{\rm A} = 2.25$, $\tilde{\mu}_{\rm B} = 1.75$, and $\tilde{L_x} = 1.0 \times 10^4$. The coefficient $\tilde{C}_{\rm p}$ is (a)$\tilde{C}_{\rm p} = 6.0 \times 10^{-6}$, (b)$\tilde{C}_{\rm p} = 6.0 \times 10^{-7}$ and (c)$\tilde{C}_{\rm p} = 6.0 \times 10^{-8}$.

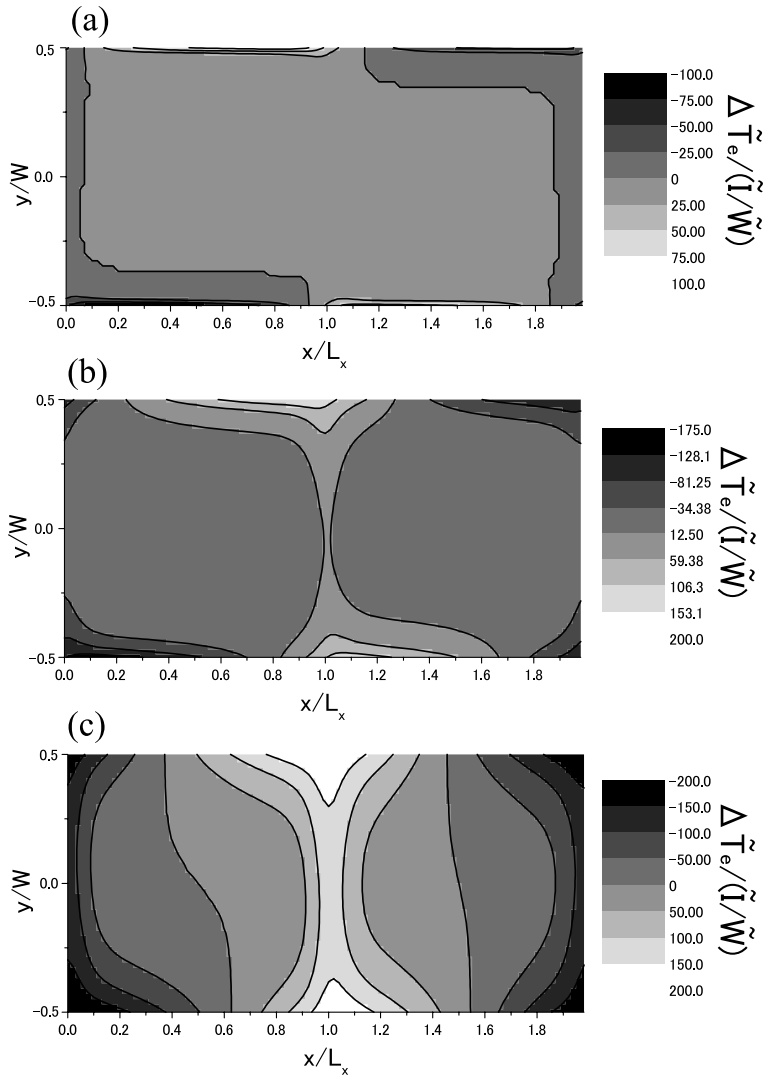

Figure 6.19: $C_{\rm p}$ dependence of the electron temperature. The spatial variations for $\tilde{L_x} = 1.0 \times 10^4$, $\tilde{W} = 0.1 \times 10^4$, $\tilde{T_{\rm L}} = 0.1$, $\tilde{\lambda} = 0.15 \times 10^4$, $\tilde{\mu}_{\rm A} = 2.25$, $\tilde{\mu}_{\rm B} = 1.75$, and $\tilde{L_x} = 1.0 \times 10^4$. The coefficient $\tilde{C}_{\rm p}$ is (a)$\tilde{C}_{\rm p} = 6.0 \times 10^{-6}$, (b)$\tilde{C}_{\rm p} = 6.0 \times 10^{-7}$ and (c)$\tilde{C}_{\rm p} = 6.0 \times 10^{-8}$.

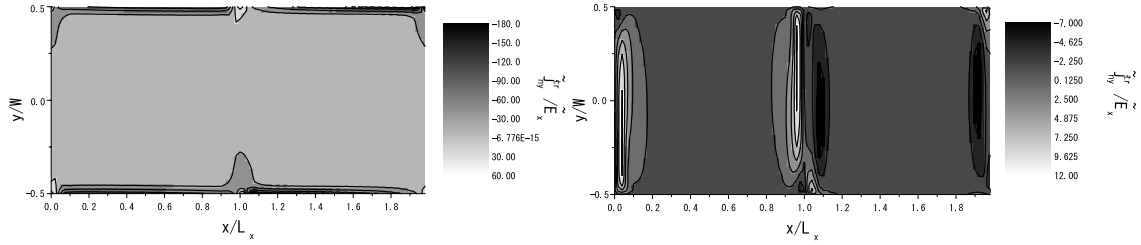

Figure 6.20: Spatial variations of $j^{\tilde{\rm tr}}_{nx}$ and $j^{\tilde{\rm tr}}_{ny}$ for $\tilde{\mu}^{\rm eq}_{\rm ec} = 3.25$, $\Delta\tilde{V} = 1.0$, $\tilde{L_x} = 1.0 \times 10^4$, $\tilde{W} = 0.1 \times 10^4$ $\tilde{\lambda} = 0.1 \times 10^4$, $N = 50$ and $\tilde{T_{\rm L}} = 0.1$.

6.3 Discussion

In this chapter, I investigated the system with potential steps. The variation of the electrochemical when $T_{\rm e} = T_{\rm L}$ shows the variation peculiar to the two-dimensional system:the electric field concentrates near the hot spot. From the numerical result on the width dependence, it has been shown that two-dimensional variation occurs in the region of $W/\lambda \geq 1$. When W is very small or λ is very long, The numerical calculation in the limit of $C_{\rm p} \to \infty$ is in agreement with the analytical calculation in the limit of $C_{\rm p} \to \infty$. The distribution of the electron temperature also has such a dependence on W/λ.

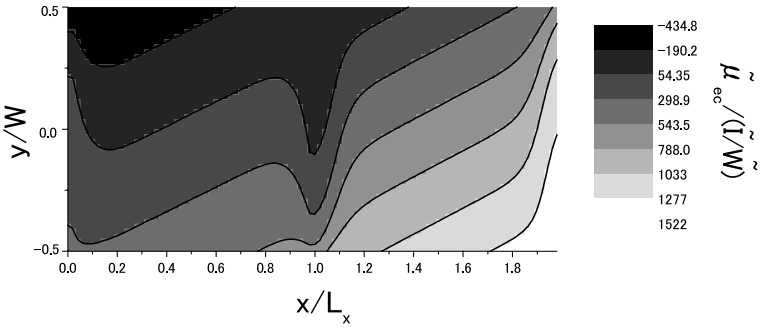

Figure 6.21: Spatial variation of $\mu_{\rm ec}$ in the limit of $C_{\rm p} \to \infty$ in the following parameters : $\tilde{\mu}_A^{\rm eq} = 3.25$, $\tilde{\mu}_B^{\rm eq} = 2.25$, $\tilde{L_x} = 1.0 \times 10^4$, $\tilde{W} = 0.1 \times 10^4$ $\tilde{\lambda} = 0.1 \times 10^4$, $N = 50$ and $\tilde{T_{\rm L}} = 0.1$.

Fig.6.21 shows that the electric field concentrates near hot spots in the limit of $C_{\rm p} \to \infty$. The thermal flux in the limit of $C_{\rm p} \to \infty$ flows as shown in Fig.6.22. The thermal flux concentrates near hot spots. The divergence of the thermal flux is large near hot spots as shown in Fig.6.23. Therefore when $C_{\rm p}$ is finite, the electron temperature becomes high near the hot spot from the equation of the energy conservation (see eq.4.4).

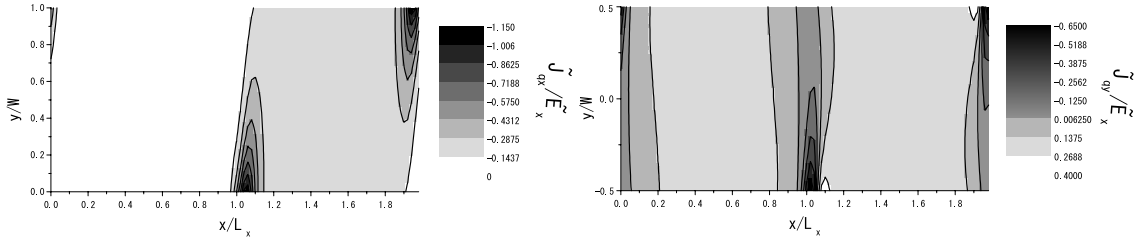

Figure 6.22: Spatial variations of $\tilde{j_{qx}^{\rm tr}}$ and $\tilde{j_{qy}^{\rm tr}}$ in the limit of $C_{\rm p} \to \infty$ for $\tilde{\mu}_A^{\rm eq} = 3.25$, $\tilde{\mu}_B^{\rm eq} = 2.25$, $\tilde{L_x} = 1.0 \times 10^4$, $\tilde{W} = 0.1 \times 10^4$ $\tilde{\lambda} = 0.1 \times 10^4$, $N = 50$ and $\tilde{T_{\rm L}} = 0.1$.

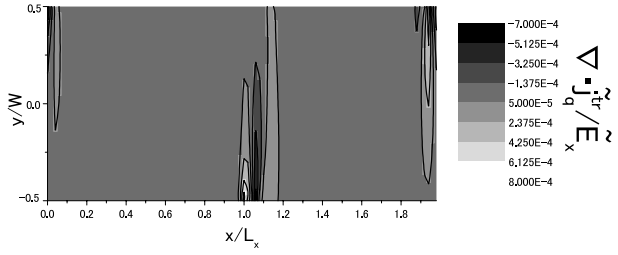

Figure 6.23: Divergence of the thermal flux in the limit of $C_{\rm p} \to \infty$.

Chapter 7

Summary

In this thesis, I have investigated the electron temperature distribution in the system which has potential steps parallel to the current by the equations of thermohydrodynamics, and clarified how the electron temperature distribution depends on various physical variables in this system.

The calculated result shows that the gradient of the electron temperature and the electric field are large near the point of intersection between the sample edge and the potential step. We found that the large gradient of the electron temperature near this point is understood by the large divergence of the thermal flux in the limit of $C_{\rm p} \to \infty$ (see eq.(4.4)). By the numerical and analytical calculation, I have investigated the width dependence of the electron temperature distribution. We found that the large gradient of the electron temperature near the point appears when W/λ is large.

I have also investigated the system without potential steps. I have shown analytically that the gradient of the electron temperature affects the diagonal resistivity as a function of the chemical potential. The diagonal resistivity shows a local maximum between the neighboring Landau levels when W is small.

The reason why the electric field concentrates near the hot spot is not clear yet. It is an interesting future problem to make clear what causes the electric field to concentrate near the hot spot.

Here, I have investigated the system which has the discontinuous confining potential in the direction perpendicular to the current. Maeda [18] has investigated the electron temperature distibution in the system which has the smooth confining potential, and has shown that the sign of the gradient of the electron temperature varies in the direction perpendicular to the current. Therefore it is interesting to investigate a system with the smooth confining potential and potential steps along the current.

Appendix

Analytical Result in the Limit of $W \ll \lambda_T$: Discontinuous Potential-Step

Model

I consider the potential which changes discontinuously in the boundary line. In the limit of $\lambda_T \gg W$, the electron temperature distribution can be derived analyticaly. I calculate the fluxes in the first-order of W since the width of the sample W is small compared with the length scale of variations of $T_{\rm e}$ and $\mu_{\rm ec}$. By using the Taylar expansion, $j^{\rm tr}_{ny}$ and $j^{\rm tr}_{qy}$ are written in this approximation as

$$j^{\rm tr}_{ny} \sim j^{\rm tr}_{ny}|_{y=W/2}, \tag{7.1}$$
$$j^{\rm tr}_{qy} \sim j^{\rm tr}_{qy}|_{y=W/2}. \tag{7.2}$$

Using the boundary conditions at $\pm W/2$, I obtain

$$j^{\rm tr}_{ny} = 0,\ -W/2 < y < W/2, \tag{7.3}$$
$$j^{\rm tr}_{qy} = 0,\ -W/2 < y < W/2. \tag{7.4}$$

Derivation and Solution

I use eq.(7.3) and eq.(7.4) to elimeinate $\nabla_y \mu_{\rm ec}$. Then I obtain

$$T_{\rm L}^{-1}\nabla_y T_{\rm e} = -\frac{A}{C}\nabla_x \mu_{\rm ec} - \frac{B}{C}T_{\rm L}^{-1}\nabla_x T_{\rm e}, \tag{7.5}$$

with

$$A = L^{11}_{yx}L^{21}_{yy} - L^{21}_{yx}L^{11}_{yy}, \tag{7.6}$$
$$B = L^{21}_{yx}L^{21}_{yy} - L^{22}_{yx}L^{11}_{yy}, \tag{7.7}$$
$$C = (L^{21}_{yy})^2 - L^{11}_{yy}L^{22}_{yy}. \tag{7.8}$$

Similarly, I use eq.(7.3) and eq.(7.4) to elimenate $\nabla_y T_{\rm e}$. Then I have

$$\nabla_y \mu_{\rm ec} = -\frac{D}{E}\nabla_x \mu_{\rm ec} - \frac{F}{E}T_{\rm L}^{-1}\nabla_x T_{\rm e}, \tag{7.9}$$

with

$$D = L^{11}_{yx}L^{22}_{yy} - L^{21}_{yx}L^{11}_{yy}, \tag{7.10}$$
$$E = L^{11}_{yy}L^{22}_{yy} - (L^{21}_{yy})^2, \tag{7.11}$$
$$F = L^{21}_{yx}L^{22}_{yy} - L^{21}_{yy}L^{22}_{yx}. \tag{7.12}$$

Using eq.(7.5) and eq.(7.9), $j_{nx}^{\rm tr}$ and $j_{qx}^{\rm tr}$ can be written as

$$
\begin{aligned}
j_{nx}^{\rm tr} &= -G_n \nabla_x \mu_{\rm ec} - H_n T_{\rm L}^{-1} \nabla_x T_{\rm e}, && (7.13)\\
j_{qx}^{\rm tr} &= -G_q \nabla_x \mu_{\rm ec} - H_q T_{\rm L}^{-1} \nabla_x T_{\rm e}, && (7.14)
\end{aligned}
$$

with

$$
\begin{aligned}
G_n &= L_{yy}^{11} + \frac{D}{E} L_{yx}^{11} + \frac{A}{C} L_{yx}^{21}, && (7.15)\\
H_n &= L_{yy}^{21} + \frac{F}{E} L_{yx}^{11} + \frac{B}{C} L_{yx}^{21}, && (7.16)\\
G_q &= L_{yy}^{21} + \frac{D}{E} L_{yx}^{21} + \frac{A}{C} L_{yx}^{22}, && (7.17)\\
H_q &= L_{yy}^{22} + \frac{F}{E} L_{yx}^{21} + \frac{B}{C} L_{yx}^{22}. && (7.18)
\end{aligned}
$$

Therefore, equations of the conservation become

$$
\begin{aligned}
-G_n \nabla_x^2 \mu_{\rm ec} - H_n T_{\rm L}^{-1} \nabla_x^2 T_{\rm e} &= 0, && (7.19)\\
-G_q \nabla_x^2 \mu_{\rm ec} - H_q T_{\rm L}^{-1} \nabla_x^2 T_{\rm e} + P_{\rm L} &= 0, && (7.20)
\end{aligned}
$$

using $\boldsymbol{\nabla} \cdot \boldsymbol{j}_n^{\rm tr} = \nabla_x j_{nx}^{\rm tr}$ and $\boldsymbol{\nabla} \cdot \boldsymbol{j}_q^{\rm tr} = \nabla_x j_{qx}^{\rm tr}$. I use eq.(7.19) and eq.(7.20) to derive differential equations. Then I obtain the equation for $T_{\rm e}(x)$:

$$
\frac{K_T}{T_{\rm L}} \nabla_x^2 T_{\rm e} = C_{\rm p}(T_{\rm e} - T_{\rm L}), \tag{7.21}
$$

with

$$
K_T = H_q - H_n (G_n)^{-1} G_q. \tag{7.22}
$$

Similarly, the equation for $\mu_{\rm ec}(x)$ is obtained:

$$
K_\mu \nabla_x^2 \mu_{\rm ec} = C_{\rm p}(T_{\rm e} - T_{\rm L}), \tag{7.23}
$$

with

$$
K_\mu = G_q - G_n (H_n)^{-1} H_q. \tag{7.24}
$$

Using eq.(7.21) and eq.(7.23), general solutions of $T_{\rm e}$ and $\mu_{\rm ec}$ in each region A and B (see Fig.4.1) are derived :

$$
\begin{aligned}
T_A(x) - T_{\rm L} &= M_1 e^{\alpha_A x} + M_2 e^{-\alpha_A x}, && (7.25)\\
T_B(x) - T_{\rm L} &= M_3 e^{\alpha_B x} + M_4 e^{-\alpha_B x}, && (7.26)\\
\mu_{\rm ecA} &= K_{nA}(T_A - T_{\rm L}) + N_1 x + N_2, && (7.27)\\
\mu_{\rm ecB} &= K_{nB}(T_B - T_{\rm L}) + N_3 x + N_4, && (7.28)
\end{aligned}
$$

with

$$
\begin{aligned}
\alpha &= \sqrt{\frac{C_{\rm p}}{K_T} T_{\rm L}}, && (7.29)\\
K_n &= \frac{K_T}{K_\mu T_{\rm L}}. && (7.30)\\
& && (7.31)
\end{aligned}
$$

To solve these equations, I use the boundary conditions :

$$
\begin{aligned}
T_{\rm e}(+0) &= T_{\rm e}(2L_x - 0), && (7.32)\\
T_{\rm e}(L_x + 0) &= T_{\rm e}(L_x - 0), && (7.33)\\
\mu_{\rm ec}(+0) &= \mu_{\rm ec}(2L_x - 0) - \mu^0_{\rm ec}, && (7.34)\\
\mu_{\rm ec}(L_x + 0) &= \mu_{\rm ec}(L_x - 0), && (7.35)\\
j^{\rm tr}_{nx}(L_x + 0) &= j^{\rm tr}_{nx}(L_x - 0), && (7.36)\\
j^{\rm tr}_{qx}(+0) &= j^{\rm tr}_{qx}(2L_x - 0), && (7.37)\\
j^{\rm tr}_{qx}(L_x + 0) &= j^{\rm tr}_{qx}(L_x - 0), && (7.38)\\
& && (7.39)
\end{aligned}
$$

since the system is periodic and variables are continuous at $x = L_x$. N_2 can't be determined sinse the equations only contain the differential of $\mu_{\rm ec}$. Therefore solving these equations, M_1, M_2, M_3, M_4, N_1, N_3 and $N_4 - N_2$ are obtained :

$$
\begin{aligned}
M_1 &= \frac{X_3 U_4 P_3 G_{nB} \Gamma_2}{Z_1 \Gamma_2 - \Gamma_1 Z_2} \mu^0_{\rm ec}, && (7.40)\\
M_2 &= -\frac{\Gamma_1}{\Gamma_2} M_1, && (7.41)\\
M_3 &= \frac{Y_1}{Y_3} M_1 + \frac{Y_2}{Y_3} M_2, && (7.42)\\
M_4 &= M_1 + e^{-\alpha_A L_x} M_2 - e^{-\alpha_B L_x} M_3, && (7.43)\\
N_1 &= \frac{\alpha_A (O_{qA} G_{nB} - O_{nA} G_{qB})(M_1 - M_2 e^{-\alpha_A L_x}) + \alpha_B (O_{nB} G_{qB} - O_{qB} G_{nB})(M_3 e^{-\alpha_B L_x} - M_4)}{G_{nA} G_{qB} - G_{qA} G_{nB}}, && (7.44)\\
N_3 &= \frac{1}{L_x} \{ K_{nA} (e^{-\alpha_A L_x} - 1)(M_1 - M_2) + K_{nB} (M_3 + M_4)(e^{-\alpha_B L_x} - 1) - N_1 L_x - \mu^0_{\rm ec} \}, && (7.45)\\
N_4 - N_2 &= K_{nA} (M_1 + M_2 e^{-\alpha_A L_x}) + L_x (N_1 - N_3) - K_{nB} (M_3 e^{-\alpha_B L_x} + M_4), && (7.46)
\end{aligned}
$$

with

$$
\begin{aligned}
X_1 &= -(1 - e^{-(\alpha_A - \alpha_B) L_x}), && (7.47)\\
X_2 &= e^{\alpha_B L_x} - e^{\alpha_B L_x}, && (7.48)\\
X_3 &= 2 \sinh(\alpha_B L_x), && (7.49)\\
Y_1 &= U_3 - U_1, && (7.50)\\
Y_2 &= U_3 e^{-\alpha_A L_x} - U_1, && (7.51)\\
Y_3 &= U_3 (e^{-\alpha_B L_x} - 1), && (7.52)\\
U_1 &= -O_{qA} \alpha_A (1 - e^{-\alpha_A L_x}), && (7.53)\\
U_3 &= O_{qB} \alpha_B (1 - e^{-\alpha_B L_x}), && (7.54)\\
\Gamma_1 &= X_1 Y_3 - Y_1 X_3, && (7.55)\\
\Gamma_2 &= X_2 Y_3 - Y_2 X_3, && (7.56)\\
Z_1 &= 2 X_1 V_3 U_3 - (V_1 U_3 + U_1 V_3) X_3, && (7.57)\\
Z_2 &= 2 X_2 V_3 U_3 + (V_1 U_3 + U_1 V_3) X_3, && (7.58)\\
V_1 &= R_1 \alpha_A + G_{nB} K_{nA} (G_{nA} G_{qB} - G_{qA} G_{nB})(1 - e^{-\alpha_A L_x}), && (7.59)\\
V_3 &= R_2 \alpha_B e^{-\alpha_B L_x} - G_{nB} K_{nB} (G_{nA} G_{qB} - G_{qA} G_{nB})(1 - e^{-\alpha_B L_x}), && (7.60)\\
R_1 &= L_x G_{nB} \{ -O_{nA} (G_{qA} + G_{qB}) + O_{qA} (G_{nA} + G_{nB}) \}, && (7.61)\\
R_2 &= L_x G_{nB} \{ -O_{nA} (G_{qA} + G_{qB}) + O_{qA} (G_{nA} + G_{nB}) \}, && (7.62)
\end{aligned}
$$

$$O_n = G_n K_n + H_n T_{\rm L}^{-1}, \tag{7.63}$$
$$O_q = G_q K_n + H_q T_{\rm L}^{-1}. \tag{7.64}$$

Results

The variations of $T_{\rm e}$ and $\mu_{\rm ec}$ are shown in Fig.7.1 and Fig.7.2. Near the boundary ($x = L_x$), $T_{\rm e}$ rises. At the boundary, transport coefficients change discontinuously since the filling factor increases discontinuously. $j_{nx}^{\rm tr}$ has no dependence on x. Therefore dissipation of the energy causes the temperature to rise since $j_{qx}^{\rm tr}$ is different in each region.

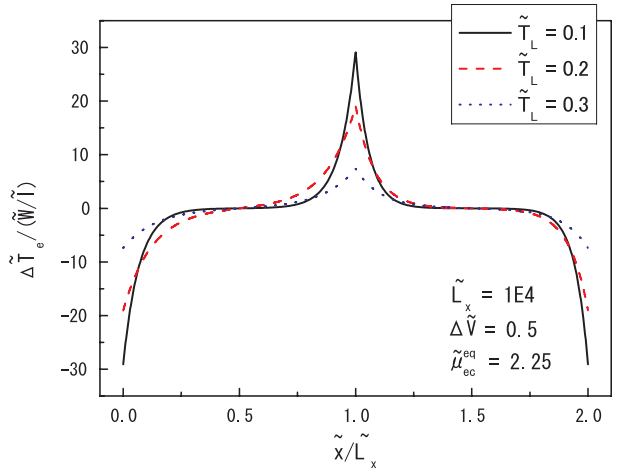

Figure 7.1: The variation of $\Delta T_{\rm e}$.

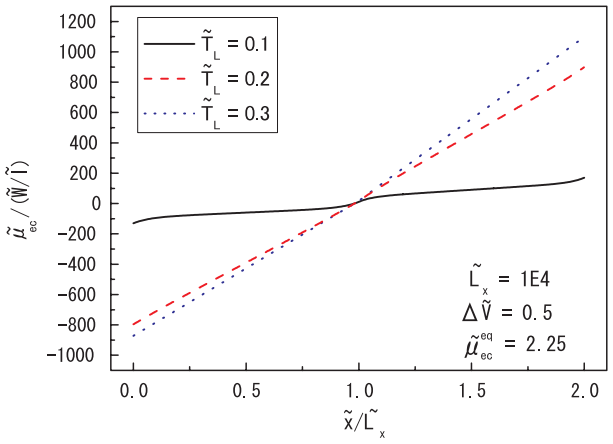

Figure 7.2: The variation of $\mu_{\rm ec}$.

Acknowlegement

Last of all, I am indebted to Professor Hiroshi Akera, an academic adviser in theoretical condensed matter physics, for his valuable guidance, constructibe criticism, fruitful discussion and accurate suggestion. I also would like to thank H. Suzuura, Y. Asano, S. Kanamaru, T. Ise, and R. Koga for valuable suggestions and discussions. Thanks Y. Kato and F. Fujimori for encourages, active help and pleasant time in the laboratory. Cordinal help and cooperation of Ms. Kumiko Kimura is also grateful acknowledged.

References

[1] G. Ebert, K. von Klitzing, K. Ploog, and G. Weimann: *J. Phys. C* **16**, 5441 (1983).

[2] A. Boisen, P. Boggild, A. Kristensen, and P. E. Lindelof: *Phys. Rev. B* **50**, 1957 (1994).

[3] S. Komiyama, T. Takamasu, S. Hiyamizu, and S. Sasa: *Solid State Commun.* **54**, 479 (1985).

[4] S. Komiyama, Y.Kawaguchi, T.Osada, and Y. Shiraki, *Phys. Rev. Lett.* **77**, 558 (1996).

[5] S. Komiyama and Y. Kawaguchi: *Phys. Rev. B* **61**, 2014 (2000).

[6] H. Akera: *J. Phys. Soc. Jpn*, **69**, 3174 (2000).

[7] H. Akera: *J. Phys. Soc. Jpn*, **70**, 1468 (2001).

[8] H. Akera: *J. Phys. Soc. Jpn*, **71**, 228 (2002).

[9] I. I. Kaya, G,Nachtwei, K. von Klitzing, and K.Eberl, *Phy. Rev. B* **58**, R7536 (1998).

[10] I. I. Kaya, G,Nachtwei, K. von Klitzing, and K.Eberl, *Physica B* **256-258**, 8 (1998).

[11] I. I. Kaya, G,Nachtwei, K. von Klitzing, and K.Eberl, *Europhysics. Lett.*, **46**, 62 (1999).

[12] I. I. Kaya, G,Nachtwei, S. Sagol. K. von Klitzing, and K.Eberl, *Physica B* **272**, 127 (1999).

[13] Cage ME, Field BF, Dziuba RF, Girvin SM,Gossard AC,Tsui DC: *Phys Rev B* **30**,2286 (1984).

[14] U. Klass, W. Dietsche, K. von Klitzing, and K. Ploog: *Surface Science.* **263** 97-99 (1992).

[15] T.Ise Master thesis (Hokkaido Univ., 2002).

[16] K. Shimoyama Master thesis (Hokkaido Univ., 2003).

[17] T. Nakagawa Master thesis (Hokkaido Univ., 2004).

[18] T. Maeda Master thesis (Hokkaido Univ., 2004)

[19] H. Akera and H. Suzuura:to be published in *J. Phys. Soc. Jpn*, **74**(2005)